

**GAIN DYNAMICS IN QUANTUM DOTS AND QUANTUM  
DASHES**

BY

**JAVEED ALI KHAN MOHAMMED**

A Thesis Presented to the  
DEANSHIP OF GRADUATE STUDIES

**KING FAHD UNIVERSITY OF PETROLEUM & MINERALS**

DHAHRAN, SAUDI ARABIA

In Partial Fulfillment of the  
Requirements for the Degree of

**MASTER OF SCIENCE**

In

**ELECTRICAL ENGINEERING**

APRIL 2012

**KING FAHD UNIVERSITY OF PETROLEUM AND MINERALS**

**DHAHRAN 31261, SAUDI ARABIA**

**DEANSHIP OF GRADUATE STUDIES**

This thesis is written by **JAVEED ALI KHAN MOHAMMED** under the direction of his thesis advisor and approved by his thesis committee members, has been presented to and accepted by the Dean of Graduate Studies, in partial fulfillment of the requirements of degree of **MASTER OF SCIENCE IN ELECTRICAL ENGINEERING**

Thesis Committee



Dr. Mohammad A. Al-Sunaidi (Advisor)  
Professor, EE Dept., KFUPM.



Dr. Ali Ahmad Al-Shaikhi  
Department Chairman



Dr. Hussain A. Al-Jamed (Member)  
Professor, EE Dept., KFUPM.



Dr. Salam A. Zummo  
Dean of Graduate Studies



Dr. Boon S. Ooi (Member)  
Professor, EE Dept., KAUST.

17/5/12

Date

## ACKNOWLEDGEMENTS

All praises and glory is to Allah, the most Merciful and the most Beneficent. I worship Him alone and I seek His forgiveness and I thank Him for my accomplishments.

I thank my advisor Dr.Mohammad A. Al Sunaidi for teaching and guiding me during my course at KFUPM. I am grateful to him for his encouragement and support, I truly learned valuable things from him. I also thank my advisor for giving me an opportunity to pursue a semester at King Abdullah University of Science and Technology (KAUST). I thank my committee members Dr.Husain Ali Al-Jamid and Dr.Boon S. Ooi for their advices and appreciations. I thank Dr. Boon S. Ooi for his support, especially during my stay at KAUST. I thank Mr. Zahed M. Khan, PhD student of Dr. Boon S. Ooi for his help and comments.

I would also like to thank my friends and fellow graduate students at KFUPM for giving me good memories worth remembering for a life time. I thank King Fahd University of Petroleum and Minerals(KFUPM) and finally I thank my family for their love and support.

All that I am or ever hope to be, I owe to my parents.

# Contents

Acknowledgments	iv
Table of Contents	v
List of Figures	ix
List of Tables	xiv
Abstract (English)	xv
Abstract (Arabic )	xvi
<b>1 Introduction</b>	<b>1</b>
1.1 Semiconductor Optical Amplifier . . . . .	3
1.2 Quantum Structures . . . . .	3
1.2.1 Quantum Well . . . . .	3

1.2.2	Quantum Dash and Quantum Dot . . . . .	4
1.3	Numerical Techniques Used . . . . .	6
1.3.1	Overview . . . . .	6
1.3.2	The FDTD Method . . . . .	7
1.4	Literature Review . . . . .	8
1.5	Thesis Objective . . . . .	12
1.6	Thesis Organization . . . . .	13
<b>2</b>	<b>Theory Of Quantum Structures</b>	<b>15</b>
2.1	Quantum Well . . . . .	16
2.2	Quantum Dash . . . . .	18
2.3	Quantum Dot . . . . .	20
<b>3</b>	<b>ADE-FDTD Solution Method</b>	<b>23</b>
3.1	FDTD Method Introduction . . . . .	23
3.2	Yee's Mesh . . . . .	24
3.3	Auxiliary Differential Equation (ADE) . . . . .	27
3.4	Stability and Dispersion Condition for ADE and FDTD . . . . .	30
3.4.1	Stability and Disperion Condition for FDTD . . . . .	30

3.4.2	Stability and Dispersion Condition in ADE-FDTD . . . . .	32
<b>4</b>	<b>Modeling of Quantum Structures</b>	<b>34</b>
4.1	Lorentzian Function as Polarization . . . . .	34
4.2	Quantum Well Modeling . . . . .	38
4.2.1	Four Level Rate Equation Model . . . . .	39
4.2.2	Discretization and ADE-FDTD Solution . . . . .	43
4.3	Quantum Dash and Dot Modeling . . . . .	47
4.3.1	Discretization and Computational Sequence . . . . .	55
<b>5</b>	<b>Simulation Results</b>	<b>58</b>
5.1	Quantum Well Results . . . . .	59
5.2	Quantum Dash and Quantum Dot Results . . . . .	68
5.2.1	Modeling Results . . . . .	68
5.2.2	Fitting Lorentzian parameters . . . . .	78
5.2.3	Dielectric waveguide . . . . .	83
<b>6</b>	<b>Conclusion and Future Work</b>	<b>90</b>
6.1	Conclusion . . . . .	91
6.2	Future Work . . . . .	92

<b>Bibliography</b>	<b>94</b>
<b>Curriculum Vitae</b>	<b>104</b>

# List of Figures

2.1	Band model for a quantum well. . . . .	17
2.2	Density of states of Bulk material(3D) Quantum Well(2D), Quantum Dash(1D) and Quantum Dot(0D) . . . . .	18
2.3	Quantum Dash structure. . . . .	19
2.4	Quantum Dashes Gaussian weighted quantum wire-like density of states (DOS). . . . .	20
2.5	Quantum Dots Gaussian weighted delta function density of states (DOS). . . . .	22
3.1	Yee's Spatial Grid Distribution of Fields . . . . .	24
3.2	Leap Frog Scheme: The Temporal Scheme of FDTD Method . . . . .	26
4.1	Maxwell's Equation Solver and Lorentz Function Computation Sequence . . . . .	37
4.2	Four level rate equation model where spontaneous and stimulated emissions occur between $E_1$ and $E_2$ . . . . .	39

4.3	Spatial location of Electric Field, Magnetic Field, Polarization and carrier Density. . . . .	44
4.4	Computation and update sequence in well. . . . .	46
4.5	Energy Diagram of Quantum Dot and Quantum Dash ensemble with wetting layer and ground states of different dot or dash groups. . . . .	48
4.6	Energy diagram of quantum dash active medium with SCH, WL and GS energy states with time constants. . . . .	49
4.7	Details on the intra dash energy levels of quantum dash density of states. . . . .	50
4.8	Computational sequence in quantum dash gain region. . . . .	56
5.1	Perfectly metallic waveguide with quantum well gain medium . . . . .	59
5.2	Real part of the complex permittivity of gain medium. . . . .	61
5.3	Imaginary part of the complex permittivity of gain medium. . . . .	62
5.4	Propagation of Gaussian pulse in the quantum well gain medium (enclosed between the vertical lines). . . . .	62
5.5	Stimulated emission in waveguide due to low amplitude input Gaussian pulse. . . . .	63
5.6	Stimulated emission in waveguide because of high amplitude input Gaussian pulse. . . . .	64
5.7	Low amplitude Gaussian pulse at point after $10\mu\text{m}$ distance inside the quantum well gain medium. . . . .	65

5.8	High amplitude Gaussian pulse at point after $10\mu\text{m}$ distance inside the quantum well gain medium. . . . .	66
5.9	Low amplitude Gain spectrum at point after $10\mu\text{m}$ distance inside the quantum well gain medium. . . . .	67
5.10	High amplitude Gain spectrum at point after $10\mu\text{m}$ distance inside the quantum well gain medium. . . . .	68
5.11	Carrier concentrations ( $N_w$ ) of wetting layer as function of time.	70
5.12	Carrier concentrations ( $N_{jk}$ ) of four different dash groups as function of time. . . . .	71
5.13	Homogeneous broadening of four different dash groups for all k ( $k = 0, 1, ..kmax$ ). . . . .	72
5.14	Carrier concentrations ( $N_{jk}$ ) of four different dash groups for all k ( $k = 0, 1, ..kmax$ ). . . . .	73
5.15	Probability of occupation ( $P_{jk}$ ) of four different dash groups for all k ( $k = 0, 1, ..kmax$ ). . . . .	74
5.16	Capture time ( $t_{cap_{jk}}$ ) of four different dash groups for all k ( $k = 0, 1, ..kmax$ ). . . . .	75
5.17	Escape time ( $t_{esc}^{jk}$ ) of four different dash groups for all k ( $k = 0, 1, ..kmax$ ). . . . .	76
5.18	Steady state InAs/InP quantum dash gain vs wavelength. . . . .	77
5.19	Steady state InAs/InP quantum dot gain vs wavelength. . . . .	77

5.20	Fitting InAs/InP quantum dash steady state gain to the Lorentzian function. . . . .	79
5.21	Real part of the complex permittivity of the quantum dash medium vs wavelength. . . . .	80
5.22	Real part of the complex permittivity of the quantum dash medium vs wavelength. . . . .	80
5.23	Fitting InAs/InP quantum dot steady state gain to the Lorentzian function. . . . .	81
5.24	Real part of complex permittivity of quantum dot medium vs wavelength. . . . .	82
5.25	Real part of complex permittivity of quantum dot medium vs wavelength. . . . .	82
5.26	Dielectric waveguide with quantum Dash/Dot gain medium. . .	83
5.27	The mode which is inserted into the dielectric waveguides. . . .	84
5.28	Gaussian pulse propagating in the dielectric waveguide with quantum dash gain medium of length $10\mu\text{m}$ . . . . .	85
5.29	Gaussian pulse propagating in the dielectric waveguide with quantum dot gain medium of length $10\mu\text{m}$ . . . . .	85
5.30	Gaussian pulse after traveling $10\mu\text{m}$ distance with and without quantum dash gain medium. . . . .	86
5.31	Gaussian pulse after traveling $10\mu\text{m}$ distance with and without quantum dot gain medium. . . . .	87

5.32	Frequency spectrum of the Gaussian pulse after traveling $10\mu\text{m}$ distance, with and without the quantum dash gain medium. . .	88
5.33	Frequency spectrum of the Gaussian pulse after traveling $10\mu\text{m}$ distance, with and without the quantum dot gain medium. . . .	89

# List of Tables

5.1	Si-nc quantum well parameters. . . . .	60
5.2	Steady state carrier concentrations in the four level model. . . . .	60
5.3	Complex permittivity parameters for quantum well. . . . .	61
5.4	InAs/InP Quantum Dash parameters. . . . .	69
5.5	Complex permittivity parameters for InAs/InP quantum dash. . . . .	79
5.6	Complex permittivity parameters for InAs/InP quantum dot. . . . .	81

## THESIS ABSTRACT

**Name:** Javeed Ali Khan Mohammed  
**Title:** Gain Dynamics in Quantum Dots and Quantum Dashes  
**Degree:** MASTER OF SCIENCE.  
**Major Field:** Electrical Department  
**Date of Degree:** April, 2012.

*In this thesis work modeling of Quantum Well, Quantum Dashes and Quantum Dots medium is done to study their gain dynamics. The Quantum well, Quantum Dashes and Dots medium are modeled using rate equations which govern carrier concentration in different levels. The effect of medium on the applied field and vice versa is studied by integrating rate equations with ADE (auxiliary differential equations)-FDTD (Finite Difference Time Domain) by means of electromagnetic polarization represented by a Lorentzian function. A time domain sequencing algorithm, consistent in time and space discretization is proposed for the modeling. The General algorithm is used to discretize ADE polarization equations of quantum well, dots and dashes medium. A coupled electromagnetic and active device model for these media is proposed to study both wave and material dynamics of the medium. A coupled model for Quantum Dots and Quantum Dashes medium is not reported so far, this thesis work is an attempt to make such a coupled model.*

## خلاصة الرسالة

الإسم: جافيد علي خان محمد

عنوان الرسالة: دينامية الإكتساب لدى النقاط الكمية و الشروط الكمية

الدرجة العلمية: ماجستير

التخصص: هندسة الكهرباء

تاريخ التخرج: إبريل, 2012 م

في هذه الدراسة, تم عمل نموذج للبئر الكمي (*Quantum Well*), الشروط الكمية (*Quantum Dashes*), و النقاط الكمية (*Quantum Dots*) وذلك لدراسة ديناميكية الإكتساب لديهم. بيئة البئر الكمي, الشروط الكمية, والنقاط الكمية تمت نمذجتها بواسطة معادلات المعدل والتي تحكم تركيز الناقل في مستويات مختلفة. تمت دراسة تأثير هذه البيئة على المجال المطبق والعكس بواسطة دمج معادلات المعدل مع المعادلات التفاضلية المساعدة (*auxiliary differential equations*) ومجال الوقت ذو الفرق المحدود من خلال إستقطاب كهرومغناطيسي ممثل بدالة لورينتزايين (*Lorentzian function*). كما تم تقديم خوارزمية متسلسلة ذات مجال وقتي تحتوي على تجزئة الوقت والفضاء للنموذج المصمم في هذه الدراسة. الخوارزمية العامة تستخدم لتجزئة إستقطاب المعادلات التفاضلية المساعدة لبيئة البئر الكمي والنقاط والشروط الكمية. كما أيضا تم إقتراح أداة كهرومغناطيسية فعالة لدراسة كلا من ديناميكية الموجة والمادة للبيئة. هذا النموذج لم يتم التطرق إليه في الدراسات السابقة وتعتبر هذه الرسالة محاولة لتقديم هكذا نموذج.

# Chapter 1

## Introduction

Since their inception the semiconductor optical amplifiers and lasers have undergone incredible amount of changes. The first semiconductor lasers were to operate at cryogenic temperatures and since then the optical amplifiers and lasers have evolved to heterostructure and to quantum semiconductors. With recent advances and flourishing of nano-photonics a lot of development has taken place in the area of directly controlling and manipulating light-matter interaction and to engineer opto-electronic properties of the semiconductor medium for light attenuation, gain and phase shift. Considerable amount of progress is being made in the engineering of optical amplifier medium and structures [1] and in quantum confined active semiconductor gain amplifiers with reduced dimensions

as in quantum wells [2], quantum dots [3] and quantum dashes or quantum wires [4].

Theoretical comprehension of the processes in optical amplifier with semiconductor gain medium in combination with numerical modeling of the semiconductor gain media is becoming the key aspect to study the process dynamics of semiconductor optical amplifier. Many elements of paramount importance have been extracted from nano-science and hence the numerical modeling of optical semiconductor amplifiers has become even more valuable and indispensable tool in understanding the various opto-electronics properties of sub-systems involved. The non linear properties and the complex nature of the coupled rate equations involved governing the nature of the gain medium makes the problem of modeling the gain medium difficult. It is evident that the numerical modeling of semiconductor optical amplifier plays a very important role in development of new structures, improvement of existing designs and introduction of novel concepts of optical amplifiers. In this work the modeling of optical semiconductor amplifiers with quantum well, quantum dot and quantum dash as gain media will be analyzed and studied.

## 1.1 Semiconductor Optical Amplifier

A semiconductor optical amplifier(SOA) is an amplifier in which amplification takes place because of semiconductor gain medium. It is like Laser diode without the mirrors that form the cavity. The signal enters the amplifier through single mode waveguide. The amplification medium of SOA is pumped electrically or optically for amplification to take place. The pumping creates a certain amount of carrier density in the conduction band which allows for the transition between conduction band to valance band. The gain occurs when the energy of the photon is just enough to simulate the transition of electron from conduction to valance band and maximum gain occurs when photon energies are slightly above the band gap [5].

## 1.2 Quantum Structures

### 1.2.1 Quantum Well

A quantum well is a thin layer which can confine (quasi-)particles (typically electrons or holes) in the dimension perpendicular to the layer surface, whereas the movement in the other dimensions is not restricted. This confinement is

called as quantum effect. It has heavy effects on the density of states of the confined particles.

### **1.2.2 Quantum Dash and Quantum Dot**

Low dimensional structures, such as quantum dashes [6; 7] and quantum dots [8], have shown enhanced optical performance in comparison with bulk and quantum well devices. Because of their large differential gain,  $\frac{\partial g}{\partial N}$  [9], and large inhomogeneously broadened spectrum, enhanced features such as a small linewidth enhancement factor, a low threshold current density, a large saturation power and ultra-fast gain recovery times [10] have been demonstrated. The strength of quantum dash and quantum dot semiconductors is the possibility to control material properties directly by geometric parameters such as dot or dash size, without changing the material composition or the macroscopic layer design. This new design parameters allow to tailor and combine material properties that are not possible with conventional technologies. For optoelectronic device applications, dot/dash-like structures allow to have a certain control on single-particle processes, like electronhole recombination or carrier relaxation processes, which has a big impact on the carrier dynamics and high speed properties of devices.

#### **Applications Dashes/Dots**

- The oldest application of quantum dots is the formation of beautiful colors in stained glasses, e.g. in church windows etc.
- Quantum dots/dashes make possible the fabrication of laser diodes with very low threshold pump power and with low temperature sensitive threshold current density.
- Quantum dots/dashes can be used in white light-emitting diodes (LEDs): they are excited with a blue or near-ultraviolet LED and emit e.g. red and green light (acting as a kind of phosphor), so that overall a white color tone is achieved.
- In semiconductor saturable absorber mirrors (SESAMs), quantum dots/dashes can serve as absorbers with a very low saturation fluence. Such quantum dots/dashes absorbers can also be contained in a glass matrix.
- Quantum dots/dashes can be parts of very sensitive photodetectors, and in the future they may function in efficient photovoltaic cells.
- In the context of quantum cryptography, quantum dots can serve as single-photon emitters.
- Quantum dots might also be suitable for performing quantum computations.

## 1.3 Numerical Techniques Used

The experimental approach for the electromagnetic analysis of light matter interaction is complicated and installation of equipments and their setup incurs huge cost. Moreover it is very difficult to experimentally measure all the possible outcomes of the system under test. As the computational power is rapidly increasing the numerical methods are becoming more efficient and accurate and hence these methods are becoming more popular among researchers and scientists. Once the numerical model of any system is perfected, it can be used as good as the experimental model. However it does not undermine the importance of the experimental analysis because the numerical models efficacy is validated with metric of experimental model.

### 1.3.1 Overview

In general numerical techniques are used in electromagnetics to solve Ordinary Differential Equations (ODE) and partial Differential Equations (PDE). A numerical method is selected for modeling of system based on its computational complexity and accuracy of the results. Some well-known electromagnetic numerical techniques or methods are : Method Of Lines (MOL), Finite Difference

Time Domain (FDTD) method, Beam Propagation Method (BPM), Finite Element Method, Monte Carlo Method, etc [11]. In this work we will use FDTD method.

### **1.3.2 The FDTD Method**

The Finite Difference Time Domain(FDTD) Method is one of the widely used computational electrodynamics modeling techniques. It is time domain method due to which it covers wide range of frequency. The FDTD central difference discretization method for Maxwell's equations for first time was presented by Yee in 1966 [12]. Since then it has been used increasingly owing to its simplicity and implementation ease. The FDTD method is such a powerful technique that its applications range from microwaves like, antennas, digital interconnects, radar signature technology, biomedical imaging, wireless communications devices, photonic crystals, biophotonics, solitons and nanoplasmonics [13]. Some of the important advantages and disadvantages of FDTD method are

#### **Advantages**

- Implementation ease and efficient for homogeneous medium.
- Treats material non-linearity naturally.

- Well developed Absorbing boundary conditions(ABC).
- Well developed Source Implementation.
- It is a traditional tool in industry.

### Disadvantages

- Cannot resolve very small details.
- Poor representation of curved boundaries.

## 1.4 Literature Review

Quantum Dashes/Dots are semiconductor nanostructures with many applications across the industries. The traditional semiconductors were evolved because of their ability to alter electrical conductivity by external stimulus of voltage or current. The quantum Dashes/Dots have all properties of traditional semiconductors and in addition to that they have the advantages of small size, fast response time, more efficient and the main difference is the peak emission frequency of quantum Dashes/Dots are sensitive to size and composition [14; 15]. Quantum confinement occurs when one or more dimensions of the quantum

structures approaches Exciton Bohr radius. The concept of conduction band, valence band and energy level still holds no longer the energy levels can be treated as continuous-they must be discrete as reported in [14; 15].

The laser with quantum well as active region was first proposed by [16]. This laser has following advantages over traditional lasers

- The confinement and nature of the electronic density of states result in more efficient devices operating at lower threshold currents than lasers with bulk active layers.
- The laser threshold current density can be reduced by decreasing the thickness of the active layer.
- Discrete energy levels gives the ability of tuning the resultant wavelength of material.
- Quantum well thickness depends on spacing between energy levels. The tuning can be achieved by changing the thickness of the well.

The inefficiencies in the quantum well lasers were removed by using new material growth capabilities such as molecular beam epitaxy in 1980's [17; 18]. Since it is possible to tune quantum Dashes/Dots structures in two/three dimensions tuning capability is higher than quantum well structures as proposed

in [19]. Quantum Dashes/Dots were proved to be more important and beneficial in comparison with quantum well structures because of low threshold current density, insensitivity of threshold current density over temperature, enhanced differential gain, high spectral purity [18].

A lot of research has been done in modeling of gain materials owing to their importance. A paper by Nagra and York [20] was one of the first to model absorbing and gain medium with ADE-FDTD, they used fully explicit discretization of the four level and two level rate equations to avoid complexities. In [21] the nonlinear-optical waveguides gate operations of femto second pulses have been studied for the first time exploiting the saturation inter-subband absorption at  $1.55 \mu\text{ m}$  in quantum wells of nitride. ADE-FDTD is used as the numerical method to study the ultra fast dynamics (1 Tb/s) of the gate operation for discretization of three level quantum rate equations proving the efficacy of the ADE-FDTD method at very high speed operations.

The dynamics of silicon based photonics [22] devices is modeled accurately by using ADE-FDTD . In this paper [22] the electromagnetic polarization is used to couple the quantum rate equation model (representing the material nonlinear properties) and classical electromagnetic wave model. The dynamics of light amplification and spontaneous emission have been analyzed with nanocrystals

(silicon) as active medium. The paper [23] is extension of [22] where the simulations tools were developed for different Si-nc (silicon nano crystal) structures and [24] is another example where PhCs are modeled with ADE-FDTD. In the paper [25] the use of ADE-FDTD is extended for the study of micro cavity optical resonators and photonic nano crystals with defects and Arnold and Ziolkowski [26] presented a different approach using Maxwell-Bloch equation using ADE-FDTD method for micro resonators. In [27] the concept of modeling quantum well is extended to Cholesteric liquid crystal (CLC) to study the circular polarization effect and amplification of light as it passes through CLC.

The paper [28] discusses about the theoretical techniques including the semiconductor Bloch equations to include dispersive and absorptive (or gain) behavior of medium using different polarization for each behavior and [29] is one of the first papers to introduce gain in Maxwell's equation using negative conductivity. The concept of introducing gain through negative conductivity and inclusion of gain saturation is extended to PhCs by Gallager, Wolfram and Payne in [30]. The papers [31; 32] describes the quantum well gain as logarithmic function [33] for gain dynamics analysis of a PhC with polarization independence. The effects homogeneous broadening of optical gain on quantum dot laser optical spectrum is proposed and discussed in [34]. A theoretical model of properties of quantum dots in linear and saturated region is presented in [35]. An expression for the

optical gain spectrum is derived for quantum dot. The modeling concept of quantum dot is extended to quantum dashes, which are difficult to model and study in [36]. In 2010 Khan [37] presented a numerical model to analyze the dynamics of carrier concentrations in InAs/InP quantum dash laser. It also include the effects of homogeneous and inhomogeneous broadening of lasing spectra.

## 1.5 Thesis Objective

The objective of the thesis is to study and analyze the gain dynamics of Quantum Well, Quantum Dots and Quantum Dashes using Finite Difference Time Domain(ADE-FDTD) simulation technique. Objectives are enumerated as follows,

- To survey the literature on the nature of Quantum Well, Quantum Dots and Quantum wires as gain medium.
- To study rate equation modeling of Quantum Well, Quantum Dots and Quantum Wires.
- To Formulate FDTD equations to include gain in the propagation media (Quantum Well, Quantum Dots and Quantum Dashes) using Auxiliary

Differential Equation (ADE) and general algorithm [38] with two dimensional Maxwell's equations.

- To use developed multidimensional simulator to study and analyze time and frequency domain dynamics.
- To extract important results.

## 1.6 Thesis Organization

The thesis is organized as follows

- Chapter 1 describes the objective of the thesis.
- Chapter 2 elucidates the theory on the nature of the quantum structures (well, dots and wires) as gain medium.
- Chapter 3 explains the numerical computational method (ADE-FDTD) which will be used to solve material rate equations and Maxwell's equations. It also discusses about the stability constraints and dispersion issues of FDTD, ADE and ADE-FDTD.
- Chapter 4 is about the rate equation modeling of these quantum structures (quantum well, quantum dots and quantum wires).

- Chapter 5 discusses the results of the models developed.
- Chapter 6 gives a prospect view about the possible extensions of this thesis as future work.

## Chapter 2

# Theory Of Quantum Structures

## 2.1 Quantum Well

A quantum well is often realized with a thin layer of a semiconductor medium, embedded between other semiconductor layers of wider bandgap (examples: GaAs quantum well embedded in AlGaAs, or InGaAs in GaAs). The thickness of such a quantum well is typically 5 to 20nm. Such thin layers can be fabricated with molecular beam epitaxy (MBE) or metalorganic chemical vapor deposition (MOCVD). Both electrons and holes can be confined in semiconductor quantum wells. In optically pumped semiconductor lasers (vertical external-cavity surface-emitting lasers), most pump radiation may be absorbed in the layers around the quantum wells, and the generated carriers are captured by the quantum wells thereafter.

If a quantum well is subject to strain, as can be caused by a slight lattice mismatch (e.g., for InGaAs quantum wells in GaAs), the electronic states are further modified, which can even be useful in laser diodes. Semiconductor quantum wells are often used in the active regions (gain medium) of laser diodes. If a large amount of optical gain or absorption is required, multiple quantum wells (MQWs) can be used, with a spacing typically chosen large enough to avoid overlap of the corresponding wave functions [39].

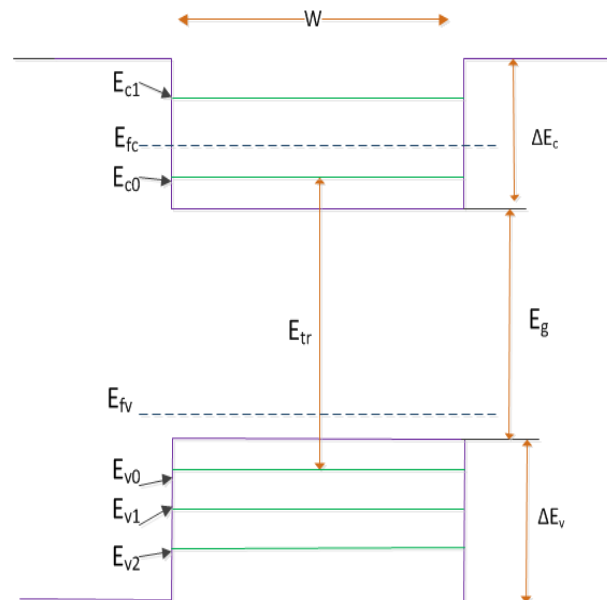


Figure 2.1: Band model for a quantum well.

A band energy diagram for a typical quantum well structure is shown in the figure(2.1). Where  $\Delta E_c$  and  $\Delta E_v$  are band edges of conduction and valence band respectively at heterojunction.  $E_{cn}$  and  $E_{vn}$  ( $n = 0, 1, 2, \dots$ ) are the quantized energy levels in conduction and valence band respectively.  $E_{tr}$  is the transition energy between two energy levels of conduction and valence band and  $E_{fc}$  and  $E_{vc}$  are the quasi-Fermi levels of electrons and holes in conduction and valence band.  $E_g$  is the band gap between conduction and valence band.

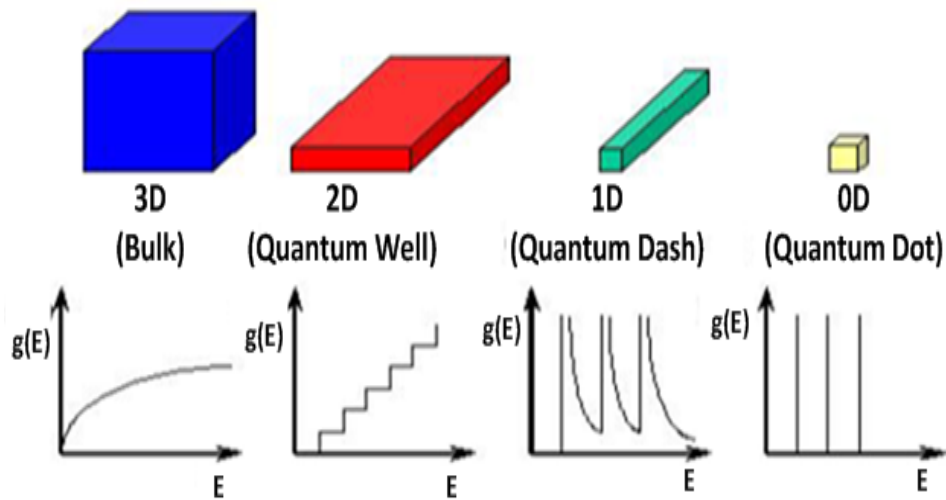


Figure 2.2: Density of states of Bulk material(3D) Quantum Well(2D), Quantum Dash(1D) and Quantum Dot(0D) .

The density of states (DOS) as function of energy for quantum well, dash and dot is shown in the figure(2.2).

## 2.2 Quantum Dash

A quantum dash is an elongated nanostructure whose cross section is similar to that of a shallow quantum dot and confines the electrons or other carriers in two dimensions. One dimensional quantum dashes are of significant interest because

they have intermediate properties between two dimensional quantum well and one dimensional quantum dot and also they can be made to operate at  $1.55\mu\text{m}$  wavelength easily [40]. Lot of research has been done in the recent past on InP based quantum dashes because of their possible applications in communications, networking and long wavelength tunning [37].

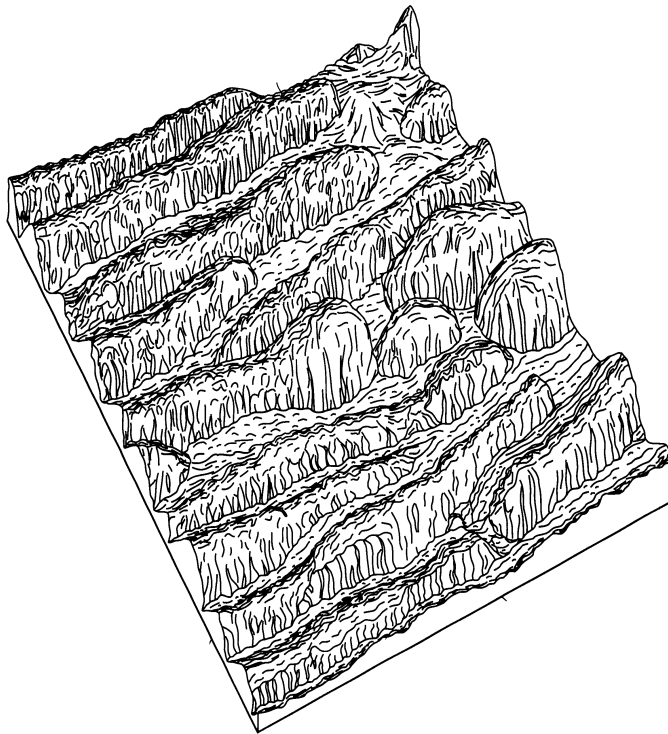


Figure 2.3: Quantum Dash structure.

The figure(2.3) shows the details of quantum dash structure . The non-uniformity in the dimensions of the Dash can be seen clearly.

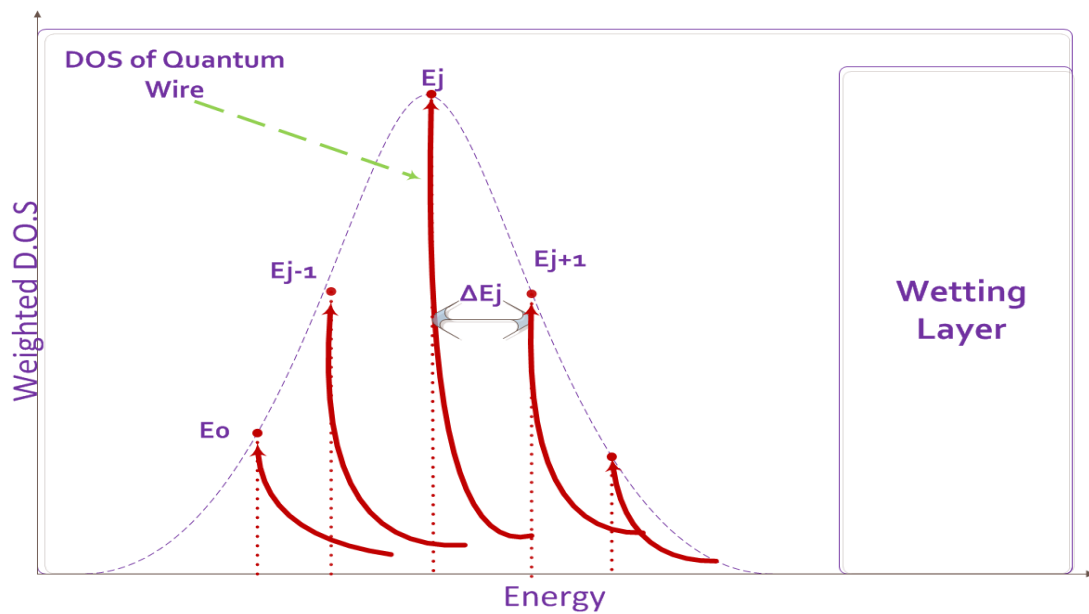


Figure 2.4: Quantum Dashes Gaussian weighted quantum wire-like density of states (DOS).

The figure(2.4) depicts the density of state diagram of a quantum dash structure. The DOS function resembles quantum wire and there is an overlap between DOS of different dash groups unlike quantum dot structure.

## 2.3 Quantum Dot

A quantum dot is a very small structure, which can confine electrons or other carriers in all three dimensions. The quantum dot quantum mechanically con-

finer electrons analogous to an electron in a box. It totally changes the density of states for the confined particles, compared with the density of states for particles in a larger piece of the material. For an ideal isolated quantum dot, there are discrete energy levels, corresponding to a delta-shaped density of states with no states in between the delta peaks. Such a behavior is known from atoms; in this sense, quantum dots can be considered as a kind of artificial atoms where the energy levels can be adjusted by design, e.g. by controlling the quantum dot dimensions or the material composition. In reality, large ensembles of quantum dots are normally used, and their size distribution leads to a somewhat smeared-out density of states, i.e. to inhomogeneous broadening.

Quantum dots can be fabricated from semiconductors. This can even accidentally happen when thin quantum wells are fabricated with molecular beam epitaxy (MBE) or metalorganic chemical vapor deposition (MOCVD), where some fluctuations of the thickness can occur. Under certain conditions (Stranski-Krastanov growth of a lattice-mismatched material on some substrate, e.g. InAs on GaAs), quantum dots can be grown in a self-organized fashion, so that they acquire more consistent sizes and distribution. Subsequently, they are often overgrown with the substrate material. Typical dimensions of the often pyramidally shaped quantum dots are of the order of 5 to 20 nm; quantum dots are therefore considered to be a topic of nanotechnology. Their density can be of the

order of 10<sup>9</sup> dots per square centimeter. In most cases, a large number of dots are simultaneously used in a device, although some quantum optics experiments require single quantum dots.

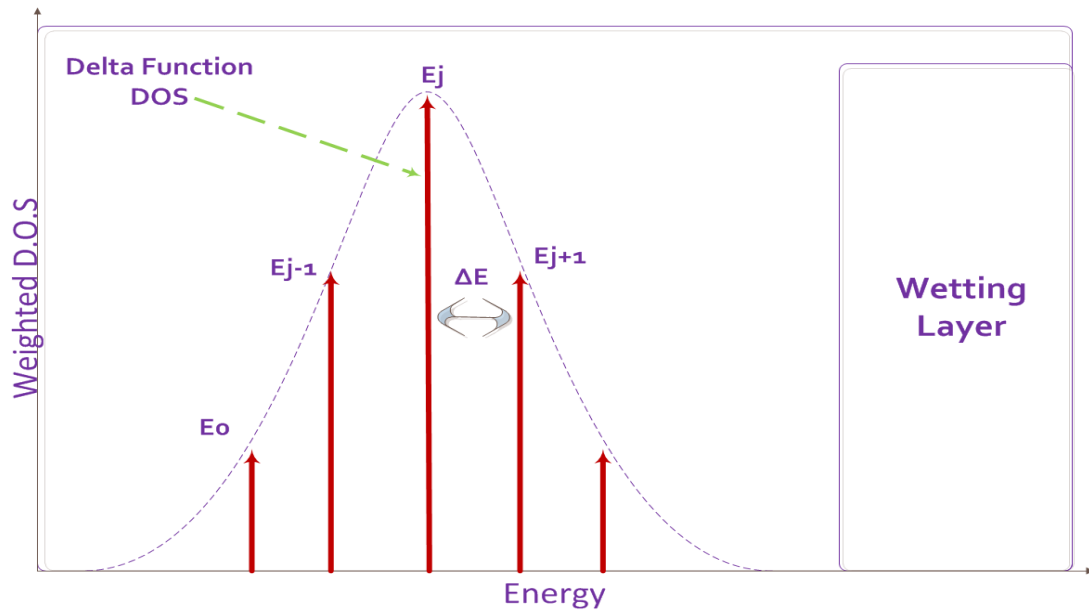


Figure 2.5: Quantum Dots Gaussian weighted delta function density of states (DOS).

The DOS of quantum dot resembles Delta function as shown in the figure(2.5).

Recently quantum Dot have attracted much attention because of the significant improvement they have shown over multiple quantum well structures because of small structure, fast carrier dynamics [40] and potential benefits such as a lower and temperature insensitive threshold current.

# Chapter 3

## ADE-FDTD Solution Method

### 3.1 FDTD Method Introduction

There are many methods available for the modeling of electromagnetic waves propagation in a medium. The methods available offer different modeling capabilities. The accuracy of these methods depends on the approximations used to simplify the Maxwell's equations. The Finite Difference Time Domain (FDTD) method is very powerful method for the numerical simulations of electromagnetic waves because it depends on direct spatial and temporal discretization of the differential equations. The FDTD technique offers appropriate and most accurate level of dynamic analysis for the ultrashort phenomena in optoelectronic,

plasmonics and photonic systems [41].

### 3.2 Yee's Mesh

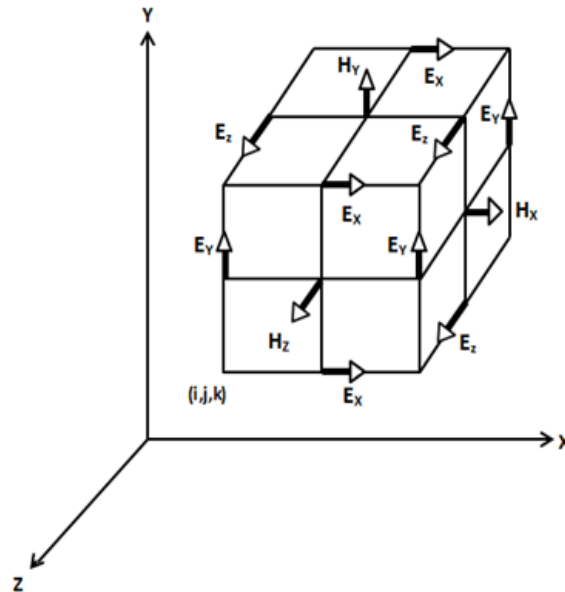


Figure 3.1: Yee's Spatial Grid Distribution of Fields

Yee's 3-Dimensional grid was proposed for structured lattices and it requires three orthogonal meshes for the electric and magnetic field as shown in figure (3.1). It positions electric field (E) and magnetic field H components at the centers of the grid lines and surfaces such that each E component is surrounded by four H components, and vice versa. This provides a neat and simple image of 3-dimensional space being filled by interlinked arrays of Ampere's law and

Faraday's law contours. It can clearly be seen that H components associated with the magnetic flux are linked with the E loops and the E components associated with the displacement current flux are linked with the H loops.

In this work Maxwell's equations are solved in two dimension for the gain dynamics analysis and in two dimensions they are reduced as

For Transverse Electric (TE) mode

$$\begin{aligned}\frac{\partial E_x}{\partial t} &= \frac{1}{\epsilon} \frac{\partial H_z}{\partial y} \\ \frac{\partial E_y}{\partial t} &= -\frac{1}{\epsilon} \frac{\partial H_z}{\partial x} \\ \frac{\partial H_z}{\partial t} &= \frac{1}{\mu} \left( \frac{\partial E_x}{\partial y} - \frac{\partial E_y}{\partial x} \right)\end{aligned}\tag{3.1}$$

For Transverse Magnetic (TM) mode

$$\begin{aligned}\frac{\partial H_x}{\partial t} &= -\frac{1}{\mu} \frac{\partial E_z}{\partial y} \\ \frac{\partial H_y}{\partial t} &= \frac{1}{\mu} \frac{\partial E_z}{\partial x} \\ \frac{\partial E_z}{\partial t} &= \frac{1}{\epsilon} \left( \frac{\partial H_y}{\partial x} - \frac{\partial H_x}{\partial y} \right)\end{aligned}\tag{3.2}$$

The partial spatial derivatives in (3.1) can be approximated by a central difference approximation in space by utilizing Yee's spatial gridding scheme the discretization is as follows

$$\begin{aligned}
\frac{\partial E_x}{\partial t} &= \frac{1}{\epsilon} \frac{H_z(i, j) - H_z(i, j - 1)}{\Delta y} \\
\frac{\partial E_y}{\partial t} &= -\frac{1}{\epsilon} \frac{H_z(i, j) - H_z(i - 1, j)}{\Delta x} \\
\frac{\partial H_z}{\partial t} &= \frac{1}{\mu} \left( \frac{E_x(i, j + 1) - E_x(i, j)}{\Delta y} - \frac{E_y(i + 1, j) - E_y(i, j)}{\Delta x} \right)
\end{aligned} \tag{3.3}$$

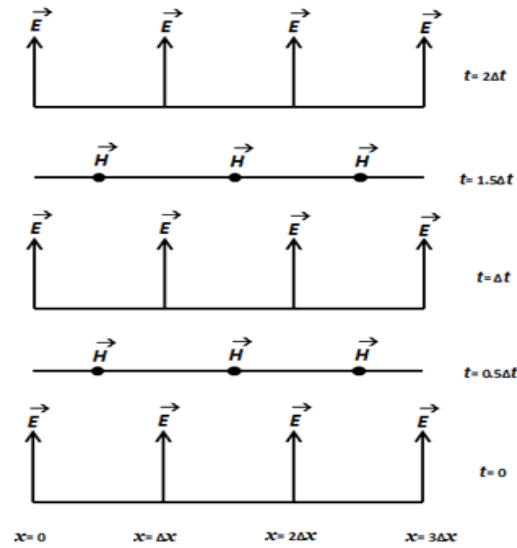


Figure 3.2: Leap Frog Scheme: The Temporal Scheme of FDTD Method

Central differencing in time for solving the E and H components is exploited again by the Yee's algorithm by using a leapfrog scheme as shown in figure(3.2).

Utilizing the previously computed values of E and the newly computed H field data, all E components in the modeled space are computed and stored in memory

for use in the next cycle. Similarly at each step, previously obtained H and the newly updated E are used to calculate the new H. This process continues until the time-stepping is completed [13].

Application of Central Difference approximation scheme to the (3.2) results in following set of equations

$$\frac{E_x^{n+1}(i+1/2, j) - E_x^n(i+1/2, j)}{\Delta t} = \frac{1}{\epsilon} \frac{H_z^{n+1/2}(i+1/2, j+1/2) - H_z^{n+1/2}(i+1/2, j-1/2)}{\Delta y} \quad (3.4)$$

$$\frac{E_y^{n+1}(i+1/2, j) - E_y^n(i+1/2, j)}{\Delta t} = -\frac{1}{\epsilon} \frac{H_z^{n+1/2}(i+1/2, j+1/2) - H_z^{n+1/2}(i-1/2, j+1/2)}{\Delta x} \quad (3.5)$$

$$\begin{aligned} & \frac{H_z^{n+1/2}(i+1/2, j+1/2) - H_z^{n-1/2}(i+1/2, j+1/2)}{\Delta t} \\ &= \frac{1}{\mu} \left( \frac{E_x^n(i, j+1) - E_x^n(i, j)}{\Delta y} - \frac{E_y^n(i+1, j) - E_y^n(i, j)}{\Delta x} \right) \end{aligned} \quad (3.6)$$

The stability and dispersion conditions of these equations is discussed in the section (3.4).

### 3.3 Auxiliary Differential Equation (ADE)

The FDTD [12] is computationally powerful due to its simplicity and implementation ease. However the FDTD is applicable only to non-dispersive and isotropic medium. In case of metals, non-linear and gain materials the medium

is non-isotropic and dispersive and hence just FDTD is not sufficient for accurate modeling. Hence FDTD should be modified to simulate such medium.

There are two types of interactions between electromagnetic radiation and atoms of the medium. First is the medium effect on the field and second is the field effect on the parameters describing the medium properties. As the electromagnetic field propagates in the medium it induces time varying dipole moment in the atoms comprising medium. The atoms which are oscillating in response to the field lose energy by radiative or non-radiative process. The total field inside the medium is sum of field in the medium due to external source and fields which atoms of the medium radiates in response to the external source. Therefore total field inside the medium can be attenuated, amplified or phase shifted by the medium. Such type of medium response can be represented using electromagnetic polarization. The different parameters in polarization function represents various characteristics of the medium.

$$P(\omega) = \frac{a}{b + jc\omega - d\omega^2} E(\omega) \quad (3.7)$$

Where  $P(\omega)$  is electromagnetic polarization,  $E(\omega)$  is frequency dependent electric field and  $a$ ,  $b$ ,  $c$  and  $d$  are the polarization parameters. This material behavior can be incorporated in FDTD by either by recursive convolution (RC)

[42] or by Auxiliary Differential Equations (ADE) [13; 43].

In this work we will use Auxiliary Differential Equations (ADE) method. In ADE method the electromagnetic polarization which describes relation between electric field intensity and electric flux density is transformed from frequency domain to time domain as

$$bP(t) + cP'(t) + dP''(t) = aE(t) \quad (3.8)$$

equation (3.8) is called as auxiliary differential equation (ADE). which is then discretized accordingly to use it along with FDTD for solving maxwell's equation. The Figure(4.1) in chapter 4 shows the integration of polarization into the Maxwell's equations.

## 3.4 Stability and Dispersion Condition for ADE and FDTD

### 3.4.1 Stability and Disperion Condition for FDTD

#### Stability Condition For FDTD

The FDTD discretization of Maxwells equations causes instability in the numerical solution, causing it to accumulate with errors if the time and space discretization steps are not chosen according to the following condition for two dimensional discretization

$$\Delta t \leq \frac{1}{c} \frac{1}{\sqrt{\frac{1}{\Delta x^2 + \Delta y^2}}} \quad (3.9)$$

where  $\Delta t$ ,  $\Delta x$  and  $\Delta y$  are discretized steps in time and space respectively [44].

A different approach towards the stability of the FDTD algorithm is proposed in [45], it is based on alternating-direction implicit method. It removes the constraint of CFL (Courant Friedrich Levy) condition at expanse of computational complexity.

## Dispersion Condition For FDTD

The implementation of FDTD algorithm to solve Maxwell's equation can be viewed as embedding electromagnetic wave in a numerical ether (a numerical medium which effect of dispersive material medium). The numerical ether causes the electromagnetic propagation mode to accumulate delays and phase errors resulting in non physical effects such as pulse broadening, ringing of single pulse waveform, anisotropy and pseudo refraction. To avoid the problem of dispersion effects at a given angle of propagation the grid density per wavelength should be taken as 10(at least) [44] to resolve the principal wavelength of the propagation mode. i.e.

$$\Delta x = \Delta y \leq \frac{\lambda_p}{10} \quad (3.10)$$

where  $\lambda_p$  is the minimum wavelength resolution required in the simulation domain .

### 3.4.2 Stability and Dispersion Condition in ADE-FDTD

#### Stability Condition For ADE-FDTD

Extension of FDTD with ADE with Lorentz Dispersive media imposes further restrictive condition on the time step discretization.

$$\Delta t \leq \frac{\tau}{100} \quad (3.11)$$

where  $\tau$  is typical medium relaxation time or the minimum time scale characteristic of the medium [46], it is the minimum of incident pulse time scale or medium relaxation time scale. If the condition is not met the instability in the system amplifies the noise which contaminates the results after several thousand time steps.

#### Dispersion Condition For ADE-FDTD

For accuracy and to avoid non-physical dispersive behavior, space discretization should be

$$\Delta x = \Delta y \leq \frac{\lambda_r}{100} \quad (3.12)$$

where  $\lambda_r$  is the minimum of the medium resonant frequencies [20].

The Stability and Dispersion conditions for ADE are more restrictive than of than the Stability and Dispersion conditions of FDTD. Being more restrictive ensure greater accuracy of FDTD solution. The ADE-FDTD system together is more dispersive than the standard FDTD and the accuracy of the system depends on how well ADE-FDTD resolves smallest time scale and wavelength in the system [46].

# Chapter 4

## Modeling of Quantum Structures

### 4.1 Lorentzian Function as Polarization

Lorentzian and Debye models are used extensively as polarization function for non-linear, non-isotropic and dispersive medium modeling. It is shown in [47] by selecting appropriate parameters number of materials (non-linear, non-isotropic and dispersive medium) can be modeled by using set of Lorentzian functions. Since media with complex  $\epsilon(\omega)$  cannot be modeled using FDTD in Maxwell's equations as discussed previously, special schemes are needed for FDTD computations to proceed. In this thesis work we are using ADE method with a Lorentzian function to represent the polarization. For the FDTD simulation

to be causal in time domain, the function which models the permittivity must satisfy the Kramers-Kronig relation in the frequency domain [47]. The frequency dependent permittivity function or electromagnetic polarization is modeled or fitted using a Lorentzian function because it ensures causality, covers a wide range of frequency spectrum and can be used efficiently in the FDTD algorithm[47]. The complex permittivity

$$\epsilon(\omega) = \epsilon_{real}(\omega) + j\epsilon_{imag}(\omega) \quad (4.1)$$

of the gain medium is modeled using a set of Lorentzian functions. Where  $\epsilon_{real}(\omega)$  is related to the stored energy in the medium and  $\epsilon_{imag}(\omega)$  is related to the loss or gain in the medium depending on the the sign. The Lorentzian function as electromagnetic polarization can be written as

$$D(\omega) = \epsilon_o\epsilon_r + P(\omega) \quad (4.2)$$

$$P(\omega) = \frac{a}{b + jc\omega - d\omega^2}E(\omega) \quad (4.3)$$

Where  $P(\omega)$  is electromagnetic polarization,  $E(\omega)$  is frequency dependent electric field,  $D(\omega)$  is electric flux density,  $\epsilon_o$  is permittivity of free space,  $\epsilon_r$  is the relative permittivity of the medium and a, b, c and d are Lorentzian function parameters describing the polarization. The Lorentzian function in terms of

permittivity can be written as

$$\epsilon(\omega) = \epsilon_o\epsilon_r + \frac{a}{b + jc\omega - d\omega^2} \quad (4.4)$$

In the frequency domain the complex permittivity  $\epsilon(\omega)$  is modeled in Maxwell's equations through the electromagnetic polarization as given in equation(4.3) As per[38] central difference discretization of polarization in time domain results in the following update equation.

$$P^n = C_1P^{n-1} + C_2P^{n-2} + C_3E^{n-1} \quad (4.5)$$

where superscript n, n-1 and n-2 are current, first previous and second previous time steps respectively.

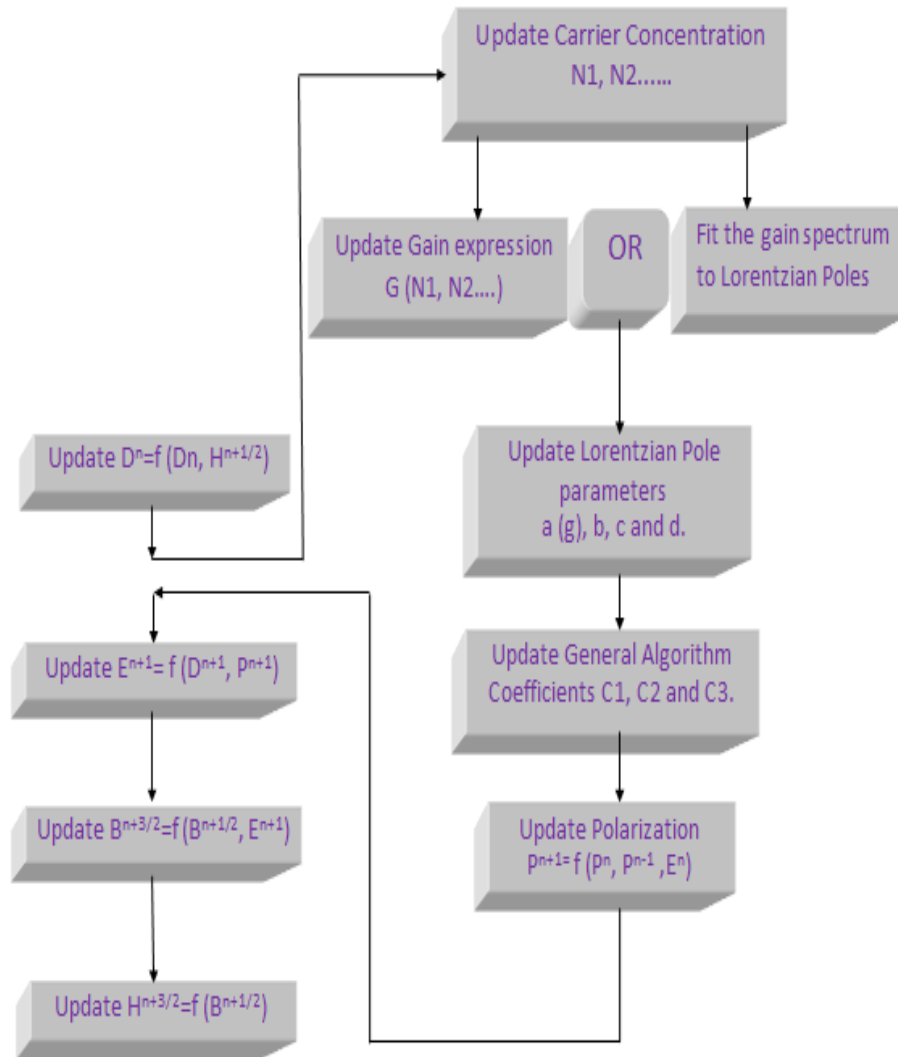


Figure 4.1: Maxwell's Equation Solver and Lorentz Function Computation Sequence

The general sequence for the numerical solution of electromagnetic Maxwell's equations and gain material polarization through Lorentzian function parame-

ters is as shown in figure(4.1).

## 4.2 Quantum Well Modeling

The physical analysis of semiconductor amplifier is determined by the optoelectronic properties of the active medium, geometry and structure. Such a medium is modeled by the using Maxwell's equations with macroscopic polarization. In case of solid state or gas it is possible to describe the active medium as a collection of amplification or absorption entities (e.g. molecules, atoms) with just two electronic energy levels; one energy level to couple resonant optical field mode and other to describe the excitation or pumping of the system [48]. In this section the focus is on modeling of quantum well, to study effects of the medium on the field and the effect of the field on the medium. There are various models to describe the physical media and the coherent process of stimulated absorption or emission [49]. In this work the modeling of a quantum well active medium is done with four level rate equation model(with two electronic energy levels as described in figure(4.2)).

### 4.2.1 Four Level Rate Equation Model

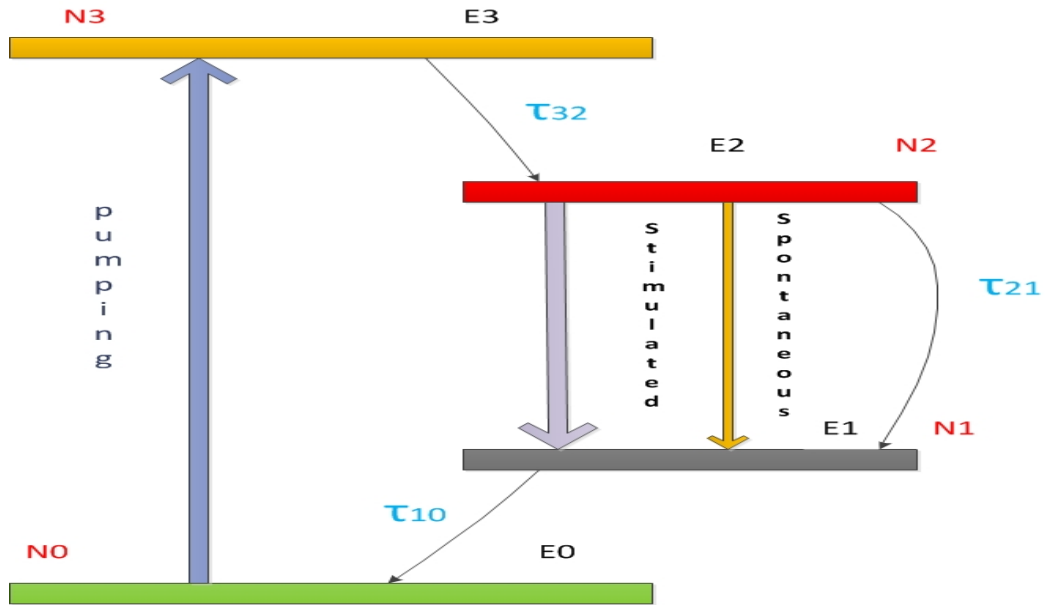


Figure 4.2: Four level rate equation model where spontaneous and stimulated emissions occur between  $E_1$  and  $E_2$ .

The carrier concentration dynamics of the four level are described by the following rate equations

$$\begin{aligned}
 \frac{dN_3(t)}{dt} &= -\frac{N_3}{\tau_{32}} + W_p N_0 \\
 \frac{dN_2(t)}{dt} &= \frac{N_3}{\tau_{32}} - \frac{N_2}{\tau_{21}} + \frac{1}{\hbar\omega_s} E(t) \cdot \frac{dP(t)}{dt} \\
 \frac{dN_1(t)}{dt} &= \frac{N_2}{\tau_{21}} - \frac{N_1}{\tau_{10}} - \frac{1}{\hbar\omega_s} E(t) \cdot \frac{dP(t)}{dt} \\
 \frac{dN_0(t)}{dt} &= \frac{N_1}{\tau_{10}} - W_p N_0
 \end{aligned} \tag{4.6}$$

where,

$N_i(i=0,1,2,3)$  is the population density of different energy levels,

$\tau_{ij}$  are life times associated with transition energy levels from  $E_i$  to  $E_j$ ,

$\omega_s$  is the central frequency of the medium associated to energy transition,

$$\omega_s = (E_1 - E_0)/\hbar,$$

$W_p$  is the pumping rate of the medium,

$\hbar$  is reduced planks constants,

and  $\frac{1}{\hbar\omega_s}E(t) \cdot \frac{dP(t)}{dt}$  is the excitation or induced radiation rate depending on the sign.

The link between the rate equation describing material properties and the electromagnetic field is made using classical electron oscillator (CEO) model [20].

The CEO model is governed by

$$\frac{d^2P(t)}{dt^2} + \gamma_{CEO} \frac{dP(t)}{dt} + \omega^2 P(t) = N \frac{e^2}{m} E(t) \quad (4.7)$$

where,

$e$  is the charge of the electron,

$m$  is mass of the electron,

$N$  is the number of electrons per unit volume,

$E_1$  and  $E_2$  are energies involved in the transition,

$\omega_a = \frac{E_2 - E_1}{\hbar}$  is the transition frequency with  $\hbar$  as reduced planks constants.  $\gamma_{CEO}$

is the classical energy decay rate given by

$$\gamma_{CEO} = \left( \frac{e^2}{m} \right) \frac{\omega_a^2}{6\pi\epsilon_0 c^3} \quad (4.8)$$

The equation(4.8) accounts for radiative energy loss using in a classical(simple) oscillating dipole model. However the real atomic transition could be different from that of a classical case. To compensate the difference between real and classical model an oscillator strength  $F_{OSC}$  is used, which is defined as

$$F_{OSC} = \frac{\gamma_r}{3\gamma_{CEO}} \quad (4.9)$$

The factor of 'three' is used because of assumption that atomic dipoles are fully aligned with the applied field, but it can be altered to incorporate a more complex condition [20]. This can be accommodated in the equation(4.7) by interchanging  $e^2/m$  with  $\kappa$ , which is defined as

$$\kappa = 3F_{OSC} \left( \frac{e^2}{m} \right) \quad (4.10)$$

Equation(4.7) assumes that atomic dipoles are oscillating in phase. The real atoms undergo dephasing which causes the destruction of coherence between

individual dipole oscillators. The real atom also loses energy from non radiative process. The total energy decay of the system can be described by linewidth of transition ( $\Delta\omega_a$ ), which is given by

$$\Delta\omega_a = \gamma_r + \gamma_{nr} + \frac{2}{T_2} \quad (4.11)$$

where  $\gamma_r, \gamma_{nr}$  and  $T_2$  are radiative, nonradiative and mean time between dephasing events.

The collective response of the atoms depends on the relative number of atoms in two energy levels and therefore the total number of oscillators in equation(4.7) can be replaced by instantaneous population difference between two energy levels, i.e.  $N \rightarrow (N_1 - N_2) = \Delta N(t)$ . With all the changes discussed above the real atomic transition can be described by modifying CEO model(4.7) to

$$\frac{d^2P(t)}{dt^2} + \Delta\omega_a \frac{dP(t)}{dt} + \omega^2 P(t) = \kappa \Delta N E(t) \quad (4.12)$$

where,

$\kappa$  is the coupling coefficient between quantum rate equation model and electromagnetic equations.

The equation(4.12) governs the polarization response of the material to the applied field and hence also called as polarization equation.

### 4.2.2 Discretization and ADE-FDTD Solution

The equation(4.6) is discretized as follows;

$$\begin{aligned}
 N_3^{n+1} &= \frac{2\tau_{32} - \Delta t}{2\tau_{32} + \Delta t} N_3^n + \left( \frac{2\tau_{32}\Delta t}{2\tau_{32} + \Delta t} \right) W_p N_0^n \\
 N_2^{n+1} &= \frac{2\tau_{21} - \Delta t}{2\tau_{21} + \Delta t} N_2^n + \frac{\tau_{21}\Delta t}{2\tau_{21} + \Delta t} \left( \frac{N_3^{n+1} + N_3^n}{\tau_{32}} \right) + \frac{\tau_{21}\Delta t}{2\tau_{21} + \Delta t} \frac{(E^{n+1} + E^n) \cdot (P^{n+1} - P^n)}{\hbar\omega_s\Delta t} \\
 N_1^{n+1} &= \frac{2\tau_{10} - \Delta t}{2\tau_{10} + \Delta t} N_1^n + \frac{\tau_{10}\Delta t}{2\tau_{10} + \Delta t} \left( \frac{N_2^{n+1} + N_2^n}{\tau_{21}} \right) - \frac{\tau_{10}\Delta t}{2\tau_{10} + \Delta t} \frac{(E^{n+1} + E^n) \cdot (P^{n+1} - P^n)}{\hbar\omega_s\Delta t}
 \end{aligned}
 \tag{4.13}$$

The  $N_0$ (ground state) is assumed to be very large in comparison to the population density in other states and hence is a constant. The spatial location of fields and carrier concentration are depicted in figure(4.3).

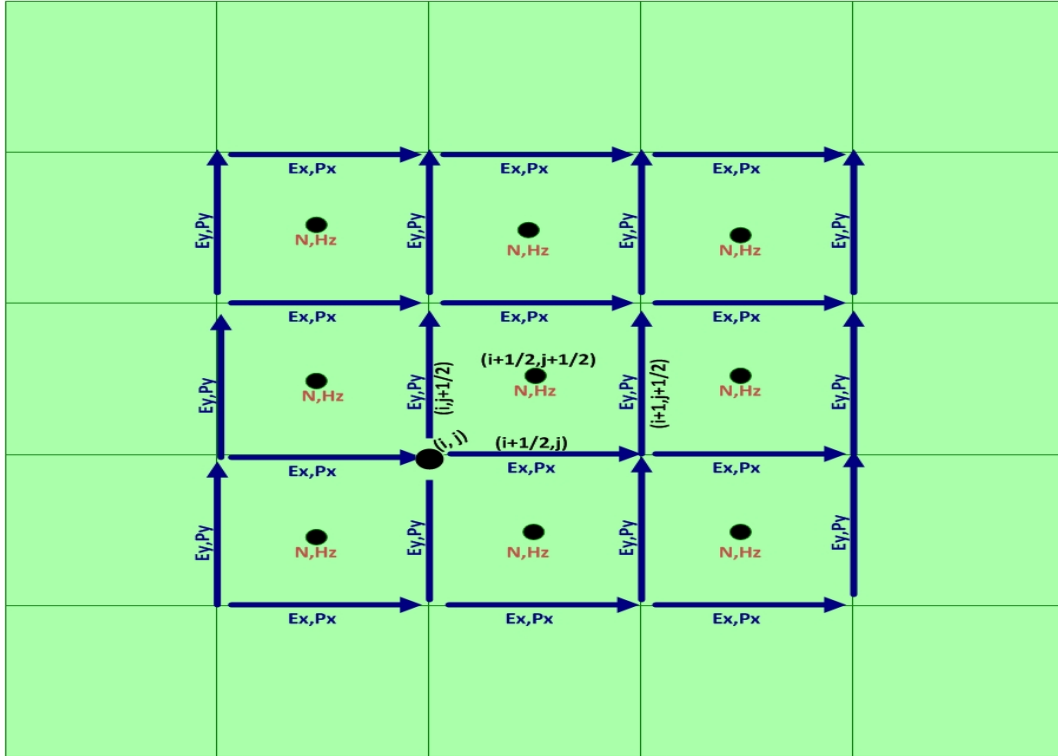


Figure 4.3: Spatial location of Electric Field, Magnetic Field, Polarization and carrier Density.

The dot product in equation(4.13) is made consistent in time by expanding it as follows

$$E^{n+1} = E_x^{n+1} \hat{a}_x + E_y^{n+1} \hat{a}_y$$

$$E^n = E_x^n \hat{a}_x + E_y^n \hat{a}_y$$

$$(E^{n+1} + E^n) \cdot (P^{n+1} - P^n) = [(E_{xavg}^{n+1} + E_{xavg}^n)(P_{xavg}^{n+1} - P_{xavg}^n) + (E_{yavg}^{n+1} + E_{yavg}^n)(P_{yavg}^{n+1} - P_{yavg}^n)] \quad (4.14)$$

Where  $\hat{a}_x$  and  $\hat{a}_y$  are unit vectors along x and y axis respectively. As the carrier concentrations  $N_i$  ( $i=0,1,2,3$ ) are defined at  $(i+1/2, j+1/2)$  the equation (4.13) is made consistent in space by defining the quantities  $E_{xavg}^n$ ,  $E_{yavg}^n$ , etc. as follows

$$\begin{aligned}
E_{xavg}^n(i+1/2, j+1/2) &= \frac{E_x^n(i+1/2, j) + E_x^n(i+1/2, j+1)}{2} \\
E_{yavg}^n(i+1/2, j+1/2) &= \frac{E_y^n(i, j+1/2) + E_y^n(i+1, j+1/2)}{2} \\
P_{xavg}^n(i+1/2, j+1/2) &= \frac{P_x^n(i+1/2, j) + P_x^n(i+1/2, j+1)}{2} \\
P_{yavg}^n(i+1/2, j+1/2) &= \frac{P_y^n(i, j+1/2) + P_y^n(i+1, j+1/2)}{2}
\end{aligned} \tag{4.15}$$

Similarly the definition of  $E_{xavg}^{n+1}(i+1/2, j+1/2)$ ,  $E_{yavg}^{n+1}(i+1/2, j+1/2)$ ,  $P_{xavg}^{n+1}(i+1/2, j+1/2)$  and  $P_{yavg}^{n+1}(i+1/2, j+1/2)$ .

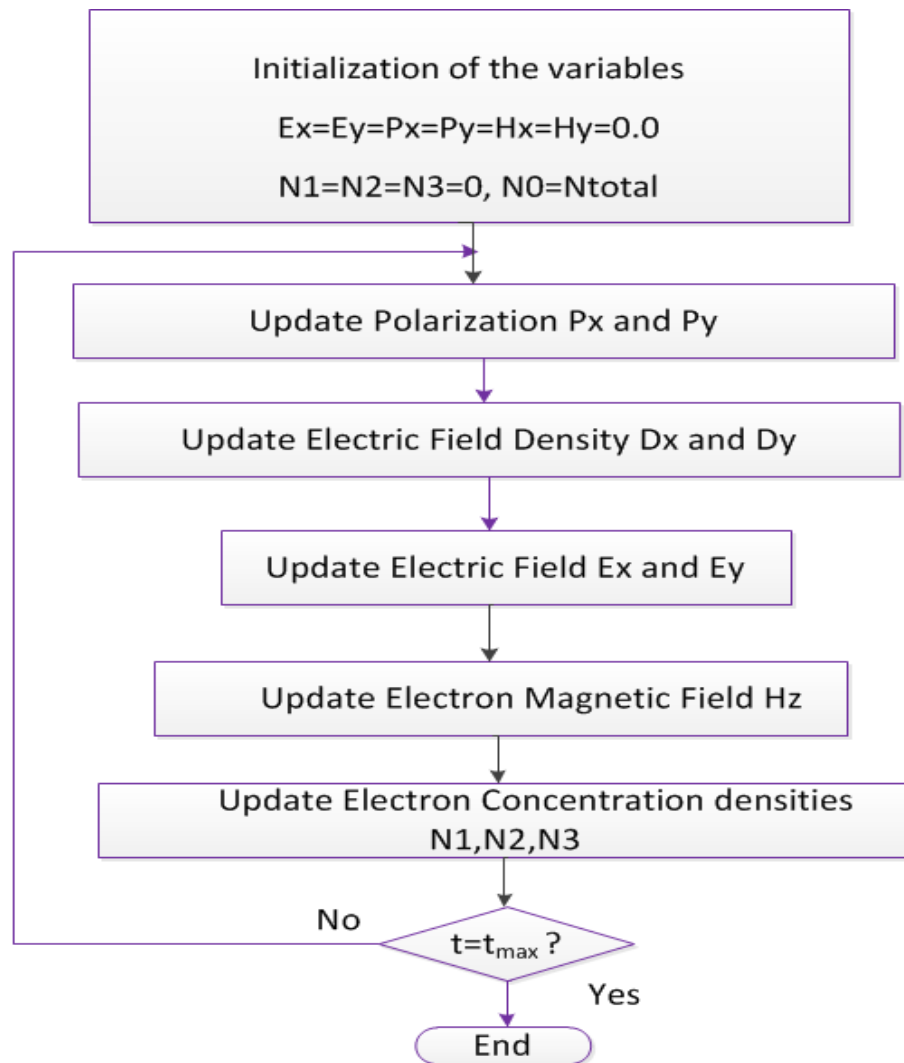


Figure 4.4: Computation and update sequence in well.

The algorithm sequence of the field, polarization and carrier concentration update for the quantum well is explained in figure(4.4).

### 4.3 Quantum Dash and Dot Modeling

Semiconductor optical amplifiers with a gain medium as quantum dash and quantum dot have outstanding characteristics in comparison with quantum well optical amplifier [50]. Quantum dots and quantum dashes are different from quantum well because of 1) inhomogeneous gain broadening because of dot and dash size (mainly because of the fluctuation in height [51]) inconsistencies in the ensembles [52; 53], which results in broader optical bandwidth when compared with quantum well 2) speedy gain recovery time which facilitates undistorted amplification of very high speed signal and 3) multi signal amplification with no cross talk [54]. Since the characteristics of quantum dash and quantum dot are fundamentally different their modeling approach is also different from that of a quantum well.

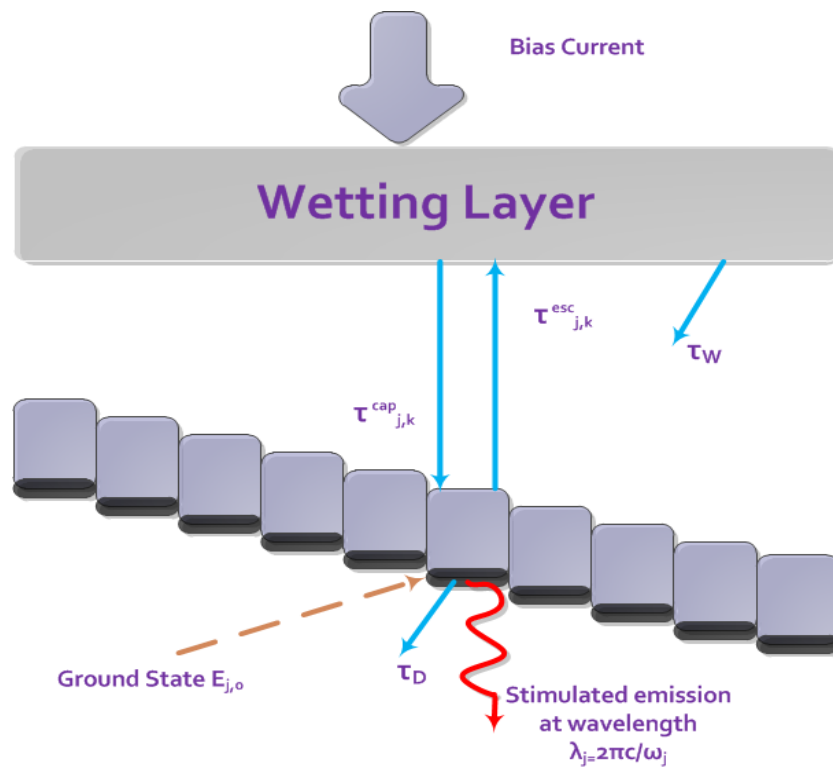


Figure 4.5: Energy Diagram of Quantum Dot and Quantum Dash ensemble with wetting layer and ground states of different dot or dash groups.

The assembly of quantum dots or dashes are divided into groups of ensembles radiating at different optical resonance peak in the spectrum.

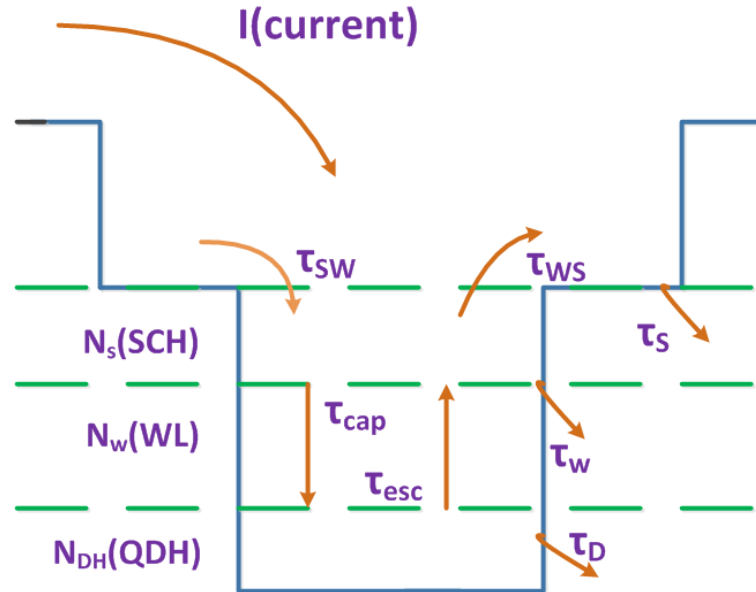


Figure 4.6: Energy diagram of quantum dash active medium with SCH, WL and GS energy states with time constants.

The gain medium of quantum dash or quantum dot semiconductor amplifier (SOA) is modeled by a system configuration that couples a gain region (dot or dash) with carrier reservoir (WL) [55; 56] as show in figure(4.5). Figure(4.6) shows the energy level diagram of a structure with separately confined heterogeneous structure (SCH), wetting layer (WL) and quantum dash energy levels. The bias current is pumped into SCH first then the current relaxes into WL and then to the quantum dash groupd state (GS). The density of states (DOS) of the quantum dot groups (each groups DOS is represented by delta function) and wetting layer (WL) is show in figure(2.5) and similarly the DOS of quantum

dash groups (each groups DOS is represented by quantum wire like DOS) and wetting layer (WL) is shown in figure(2.4).

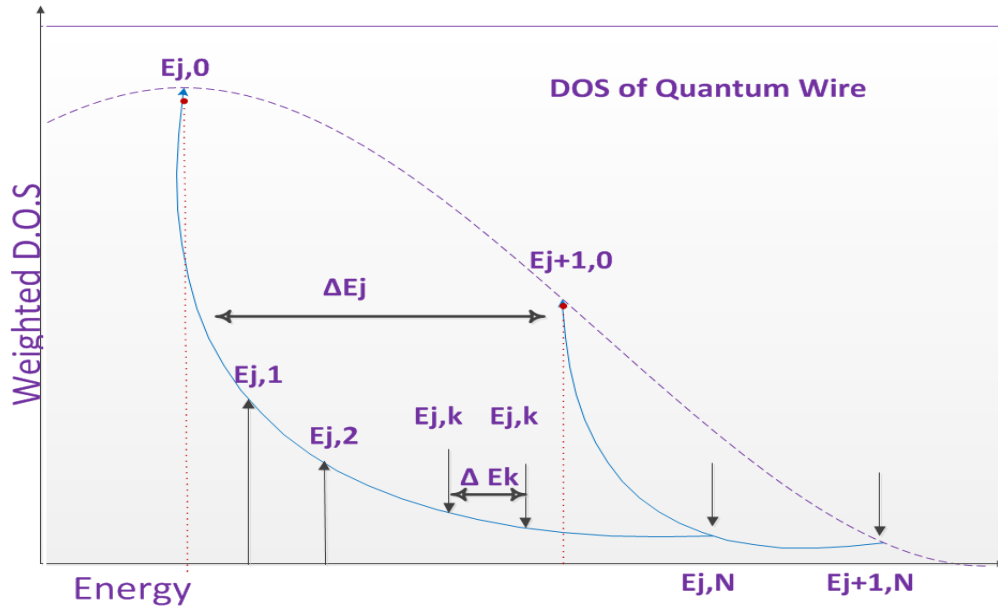


Figure 4.7: Details on the intra dash energy levels of quantum dash density of states.

Only the ground states (GS) of quantum dashes and dots are considered because no conspicuous emission is observed from the excited states because the wetting layer is energetically close to the excited states of quantum dashes or dots and hence excited carriers thermalize rapidly inhibiting emission [57].

$M$  group of quantum dashes or dots and  $N$  intra dash energy levels with  $\Delta E_j$  as energy difference between adjacent dash or dot group and with  $\Delta E_k$  intra dash energy difference are considered as for model as depicted in figure (4.7).

carrier capture and escape time from the wetting layer (WL) to the quantum dash groups are depicted in figure(4.5).

The gain in the active region of quantum dash or dot is defined by the following equation

$$g_m^{j,k} = \frac{2\pi e^2 \hbar N_D |M_{cv}|^2}{E_{cv}} (2P_{j,k} - 1) G_{j,k} B(E_m - E_{j,k}) \quad (4.16)$$

where,

$$N_D = N_{dh} \sqrt{2m_e^*/\pi^2 \hbar^2} \sqrt{E_{j,N+1} - E_{j,0}} \quad (4.17)$$

is the volumetric Density Of State (DOS) with  $N_{dh}$  as dash density cross section and  $m_e^*$  as effective mass of electron in the active region,  $|M_{cv}|^2$  is transition matrix,

$$P_{j,k} = N_{j,k}/2D_g N_D V_A G_{j,k} \quad (4.18)$$

is probability of occupation of the  $N_{j,k}$  population of carriers in the  $E_{j,k}^{th}$  dash group,

$B(E_m - E_{j,k})$  is the Lorentzian homogeneous broadening and is defined as

$$B(E_m - E_{j,k}) = \frac{\hbar \Gamma_{homg}/2\pi}{(E_m - E_{j,k})^2 + (\hbar \Gamma_{homg}/2)^2} \quad (4.19)$$

with  $\hbar \Gamma_{homg}$  as Full Width Half Maximum (FWHM), and with  $E_{j,k}$  and  $E_m$  (longitudinal

photon modes) defined as

$$E_{j,k} = E_{cv} - (M - j)\Delta E_j + k\Delta E_k \quad (4.20)$$

and with  $E_{cv}$  as central transition energy of the dash group,

$$E_m = E_{cvp} - (M - m)\Delta E_m \quad (4.21)$$

$m = 0, 1, 2, \dots, 2M_p$ ,  $E_{cvp}$  is the central photon energy mode and  $E_m = ch/2n_a L$  ( $n_a$  is active region refractive index),

$G_{j,k}$  Gaussian inhomogeneous broadening which results due to quantum dash properties fluctuations more predominantly because of height is defined as

$$G_{j,k} = \frac{1}{\sqrt{2\pi}\xi_0} \exp\left[\frac{(E_{j,0} - E_{cv})^2}{2\xi^2}\right] dE_j \frac{\sqrt{E_{j,k+1} - E_{j,0}} - \sqrt{E_{j,k} - E_{j,0}}}{\sqrt{E_{j,N+1} - E_{j,0}}} \quad (4.22)$$

(as shown in figure(2.4))

is the Gaussian inhomogeneous broadening which results due to quantum dot properties fluctuations with delta functions as DOS is defined as

$$G_{j,k} = \frac{1}{\sqrt{2\pi}\xi_0} \exp\left[\frac{(E_{j,0} - E_{cv})^2}{2\xi^2}\right] \quad (4.23)$$

(as shown in figure(2.5))

with  $\Gamma_{inhom} = 2.35\xi_0$  as FWHM and  $G_{j,k}$  is normalized ( $\sum_{j,k} G_{j,k} = 1$ ).

The carrier concentrations occupation dynamics quantum dash groups in different energy levels as shown in fig (2.4) are governed by the following equations

$$\frac{dN_w}{dt} = \frac{\eta_i I}{e} + \sum_j \sum_k \frac{N_{j,k}}{\tau_{esc}^{j,k}} - \frac{N_w}{\tau_{cap}^-} - \frac{N_w}{\tau_w} \quad (4.24)$$

$$\frac{dN_{j,k}}{dt} = \frac{N_w G_{j,k}}{\tau_{cap}^{j,k}} - \frac{N_{j,k}}{\tau_{esc}^{j,k}} - \frac{N_{j,k}}{\tau_D} - \frac{c\Gamma}{n_a} \sum_m g_m^{j,k} S_m \quad (4.25)$$

where,  $N_w$  is the carrier concentration in the wetting layer,  $N_{j,k}$  is the carrier concentrations in the different quantum dash groups as show in figure(2.4),  $\eta_i$  is internal quantum efficiency,  $I$  is the injection current,  $\tau_{cap}^-$  is the average carrier relaxation time from the wetting layer (WL) to the ground states (GS) of the different quantum dash groups,  $S_m$  is the population density of the photons,

$\tau_{cap}^{j,k}$  is the carrier relaxation time from from wetting layer to different quantum dash groups GS and is calculated as

$$\frac{1}{\tau_{cap}^-} = \sum_j \sum_k \frac{G_{j,k}}{\tau_{cap}^{j,k}} = \sum_j \sum_k \frac{(1 - P_{j,k})G_{j,k}}{\tau_{capo}} \quad (4.26)$$

$\tau_{esc}^{j,k}$  is the carrier escape time from different quantum dash groups GS to the wetting layer and is defined as

$$\frac{1}{\tau_{esc}^{j,k}} = \frac{1}{\tau_{esco}^{j,k}} \left[ 1 - \frac{N_w}{2D_w V_w} \right] \quad (4.27)$$

with the definition of  $\tau_{esco}^{j,k}$  as

$$\tau_{esco}^{j,k} = \left[ \frac{D_G N_D V_A}{D_W V_W} \right] \tau_{capo} \exp \left[ \frac{E_{WL} - E_{j,k}}{kT} \right] \quad (4.28)$$

where,  $D_G$  is the degeneracy of quantum dash GS,

$D_W$  is the volumetric density of state (DOS) of the wetting layer(WL),

$E_{WL}$  is the wetting layer (WL) energy level,

$V_A$  and  $V_W$  are the volumes of active region and wetting layer respectively and

are calculated as  $V_A = 0.75LW_{dash}h_{dash}N_{lyr}$  and  $V_{WL} = w_{WL}Lh_{WL}N_{lyr}$  with

$N_{lyr}$  as number of quantum dash stacking layers,

$h_{dash}$  and  $w_{dash}$  are the height and width of the quantum dashes respectively,

$L$  and  $W$  being the length and width of the active region,

$w_{WL}$  and  $h_{WL}$  are the width and height of the wetting layer (WL) respectively,

$k$  is the Boltzmann's constant and  $T$  is temperature of active region .

### 4.3.1 Discretization and Computational Sequence

The quantum dash rate equations(4.24,4.24) are discretized using leap frog method as follows

$$N_w^{n+1} = N_w^{n-1} + 2\Delta t \left[ \sum_j \sum_k \frac{N_{j,k}^n}{\tau_{esc}^{j,k}} - \frac{N_w^n}{\tau_{cap}^-} - \frac{N_w^n}{\tau_w} + \frac{\eta_i I}{e} \right] \quad (4.29)$$

$$N_{j,k}^{n+1} = N_{j,k}^{n-1} + 2\Delta t \left[ G_{j,k} \frac{N_w^n}{\tau_{cap}} - \frac{N_{j,k}^n}{\tau_{esc}^{j,k}} - \frac{N_w^n}{\tau_D} - \frac{c\Gamma}{n_a} \sum_m g_m^{j,k} S_m \right] \quad (4.30)$$

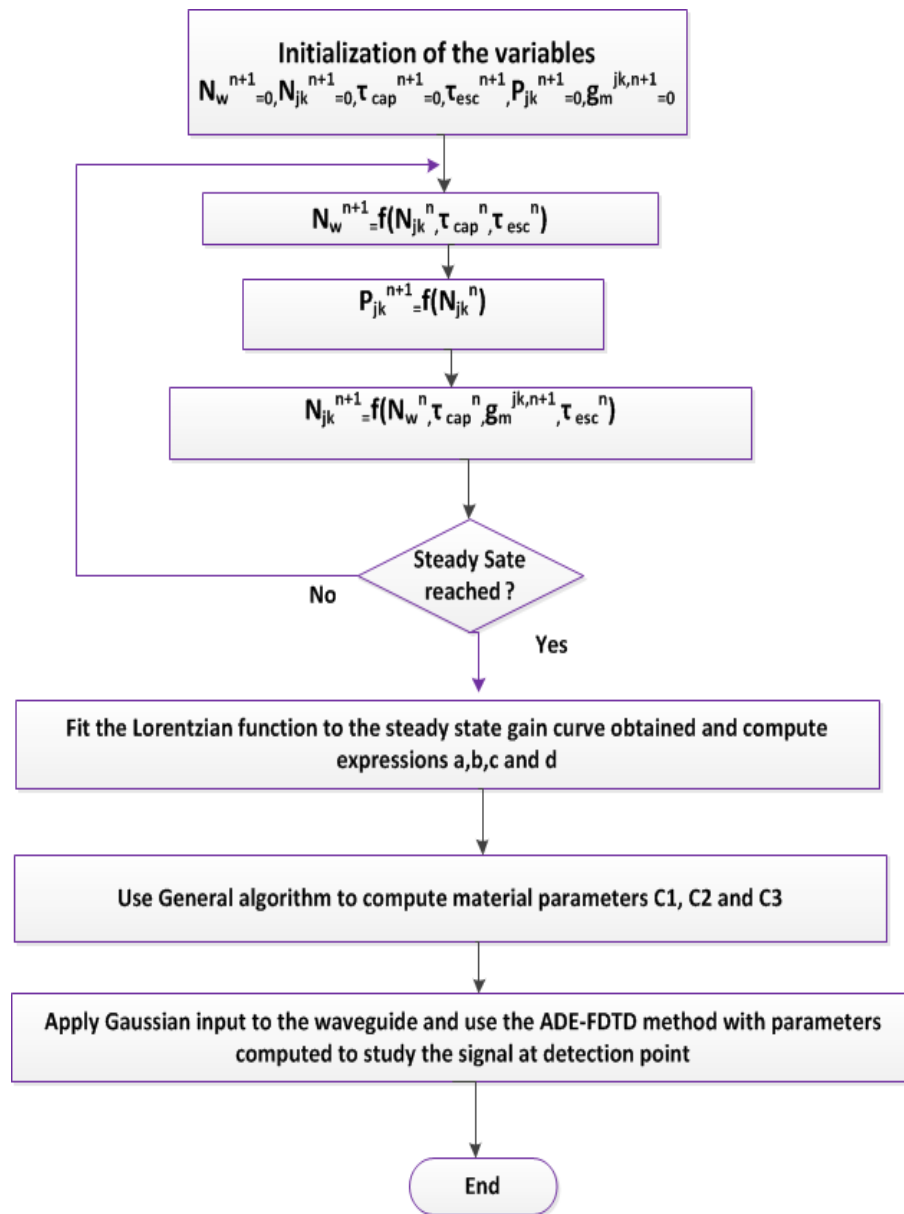


Figure 4.8: Computational sequence in quantum dash gain region.

The computation sequence to update the rate equations(4.29,4.30), to fit com-

puted gain of the quantum dash region to the Lorentzian function and to compute ADE-FDTD method with the fitted parameters are shown in figure(4.8).

# Chapter 5

## Simulation Results

## 5.1 Quantum Well Results

The quantum well gain medium is embedded in a perfectly metallic waveguide as shown in figure(5.1).

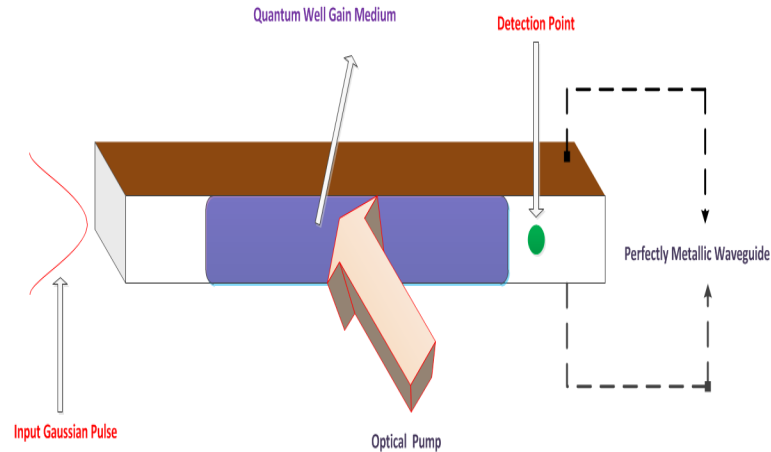


Figure 5.1: Perfectly metallic waveguide with quantum well gain medium .

The simulation parameter ([23]) of for the Si-nc (silicon nanocrystals) quantum gain medium are given in the table(5.1).

The discretized equations(4.13) with  $\Delta t = 10^{-17}s$  and with quantum well parameters mentioned in the table(5.1) are run for 1ns without input signal and following steady state carrier concentrations in four levels (as shown in 4.2) are obtained (pumping rate used is  $W_p = 1 \times 10^8 s^{-1}$ )

Table 5.1: Si-nc quantum well parameters.

Pump wavelength (nm)	532
Absorption cross-section $\sigma_p(cm^2)$	$10^{-14}$
Emission cross-section $\sigma_s(cm^2)$	$3 \times 10^{-16}$
Si-nc concentration $N_{tot}(m^{-3})$	$6 \times 10^{24}$
Emission wavelength $\lambda$ (nm)	750
Emission spectrum linewidth $\lambda_{lw}$ (nm)	200
$\tau_{10}$ (s)	$10^{-15}$
$\tau_{21}$ (s)	$10^{-5}$
$\tau_{32}$ (s)	$10^{-15}$
Refractive index of Si-ncs	$1.9 + i0.0014$
Refractive index of $SiO_2$	1.454

Table 5.2: Steady state carrier concentrations in the four level model.

<i>carrierConcentration</i>	<i>Value</i>
$N_0 (m^3)$	$6 \times 10^{24}$
$N_1 (m^3)$	$1.51115205 \times 10^{13}$
$N_2 (m^3)$	$1.51115727 \times 10^{23}$
$N_3 (m^3)$	$5.99996623E \times 10^{17}$

The real and imaginary part of complex permittivity

$$\epsilon_s = \epsilon_o \epsilon_r + \frac{a}{b + jc\omega - d\omega^2}$$

are plotted in figure(5.2) and figure(5.3) for the parameter values mentioned in the tabel(5.3).

In the table(5.3)  $n_r$  is the real part of the complex refractive index and  $N12 =$

Table 5.3: Complex permittivity parameters for quantum well.

$\epsilon_r$	$n_r^2$
a	$c\epsilon_0\sqrt{\epsilon_r}\sigma_s\Delta\omega_{lw}N_{12}$
b	$(2\pi c/\lambda)^2$
c	$2\pi c/\lambda_{lw}$
d	1

$0.91N_{tot}$  .

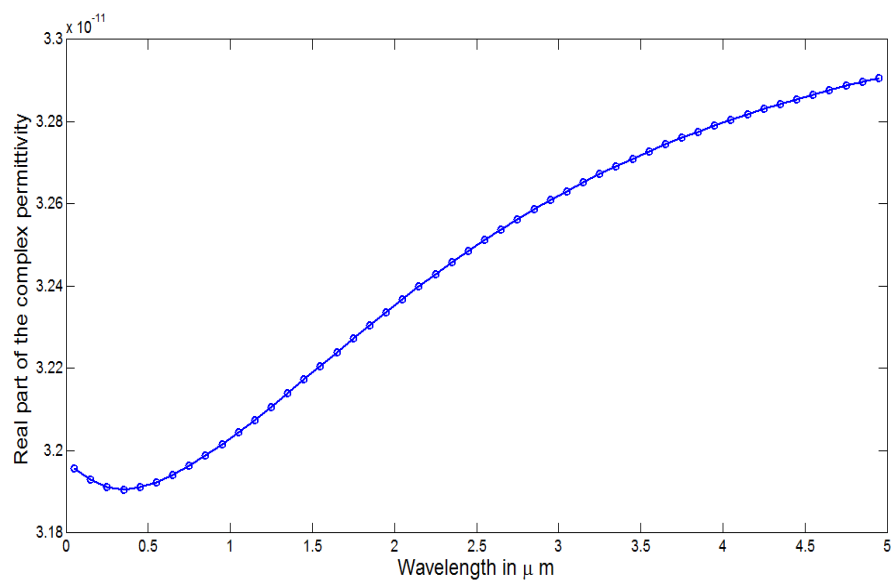


Figure 5.2: Real part of the complex permittivity of gain medium.

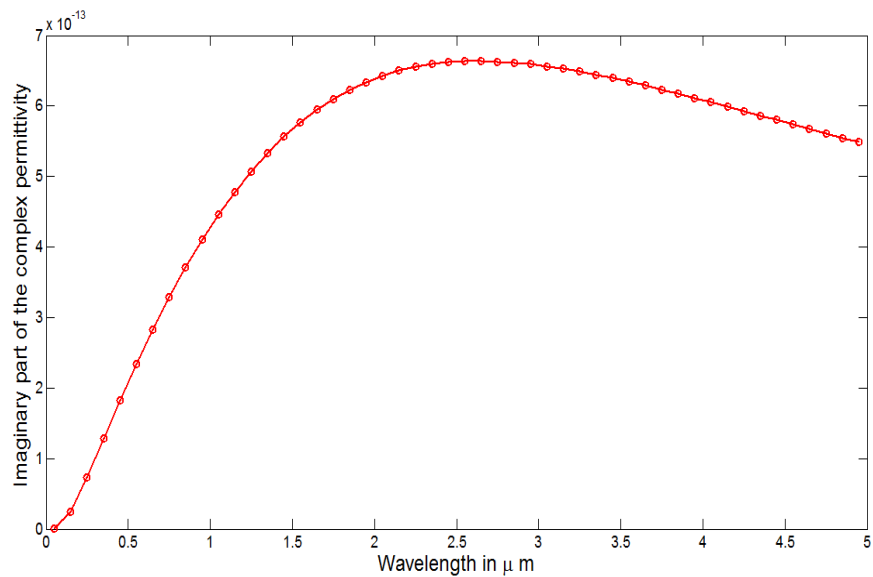


Figure 5.3: Imaginary part of the complex permittivity of gain medium.

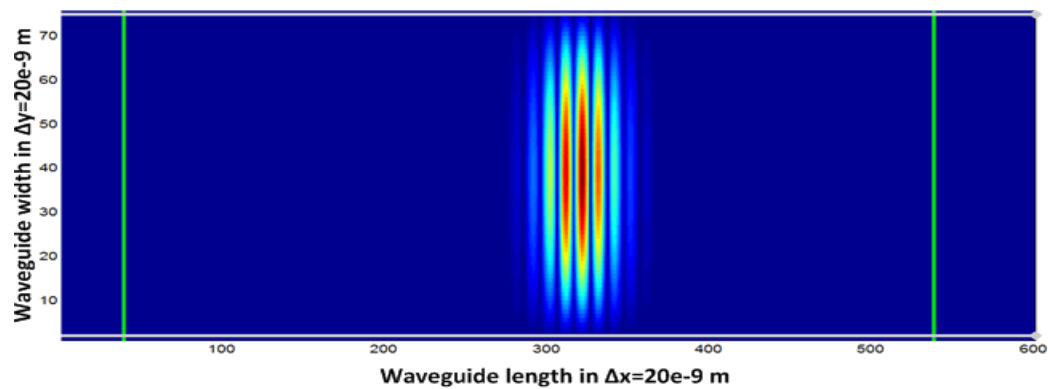


Figure 5.4: Propagation of Gaussian pulse in the quantum well gain medium (enclosed between the vertical lines).

The figure(5.5) shows the stimulated emission in the quantum well gain medium in response to the low amplitude ( $1V/M$ ) Gaussian pulse figure(5.4).

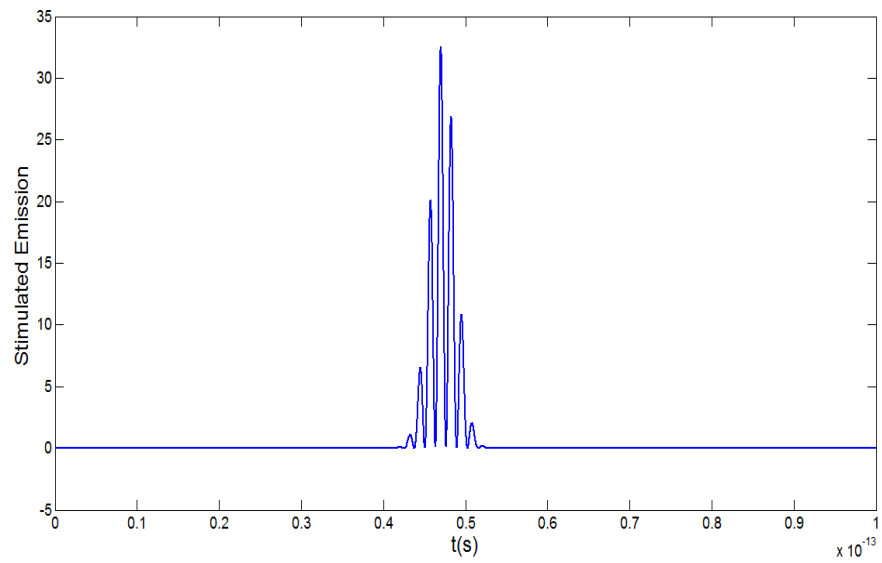


Figure 5.5: Stimulated emission in waveguide due to low amplitude input Gaussian pulse.

The amount of stimulated emission is very less to effect the carrier concentrations in the four level model and hence it does not affect the gain.

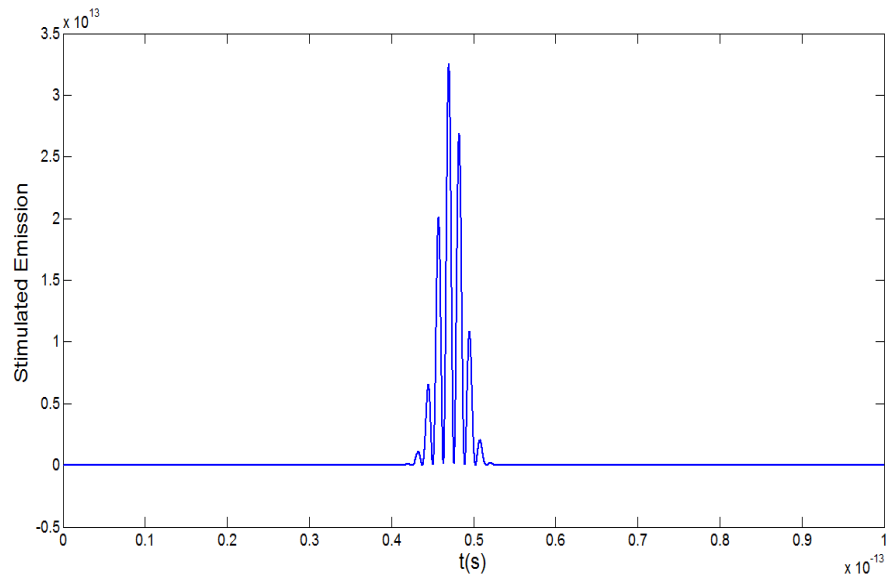


Figure 5.6: Stimulated emission in waveguide because of high amplitude input Gaussian pulse.

The stimulated emission figure(5.6) for the high amplitude ( $10^6 V/m$ ) Gaussian pulse is very high in comparison with low amplitude figure(5.5). But it is not high enough to effect the carrier concentration  $N_2$  (because  $N_2$  as shown in table(5.2) is even larger). Hence even the high amplitude Gaussian pulse does not affect the carrier levels in one pass (unlike in cavity, where multiple reflection inside the cavity makes the stimulated emission a very huge quantity).

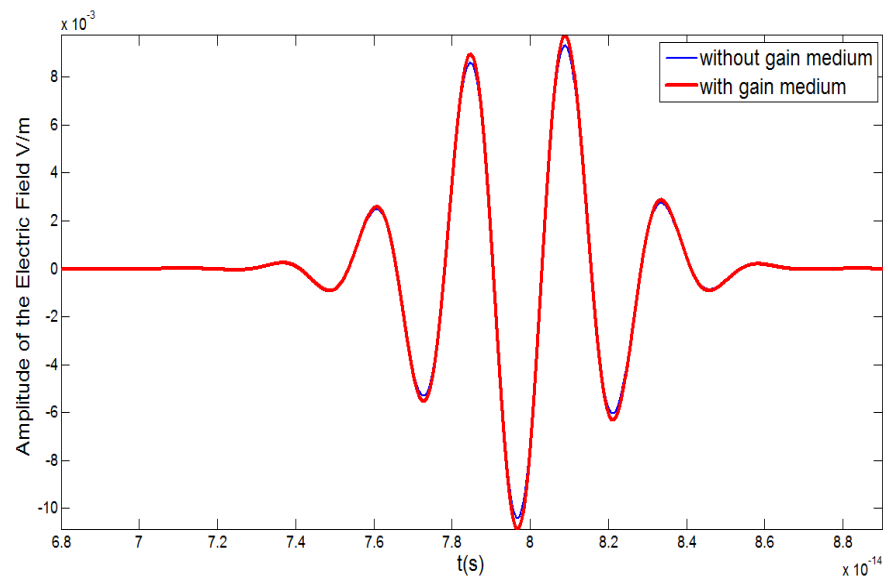


Figure 5.7: Low amplitude Gaussian pulse at point after  $10\mu\text{m}$  distance inside the quantum well gain medium.

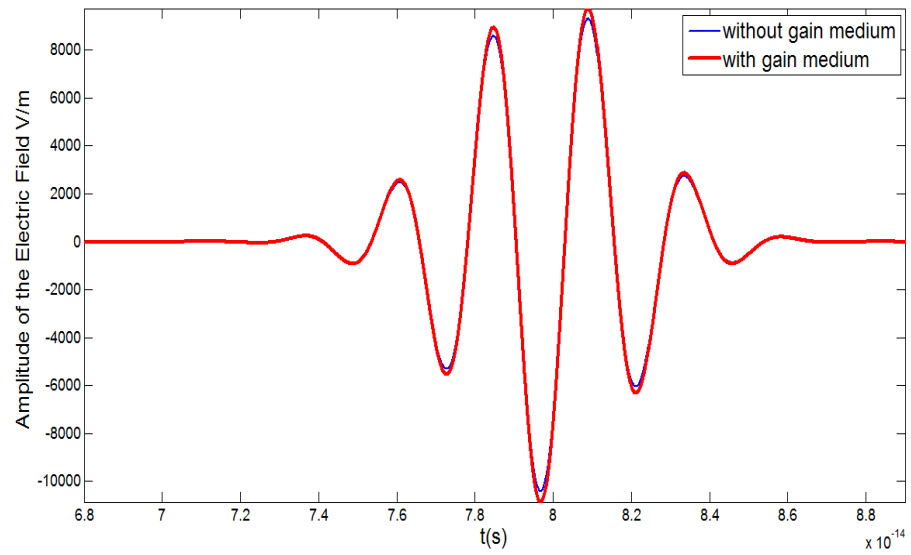


Figure 5.8: High amplitude Gaussian pulse at point after  $10\mu\text{m}$  distance inside the quantum well gain medium.

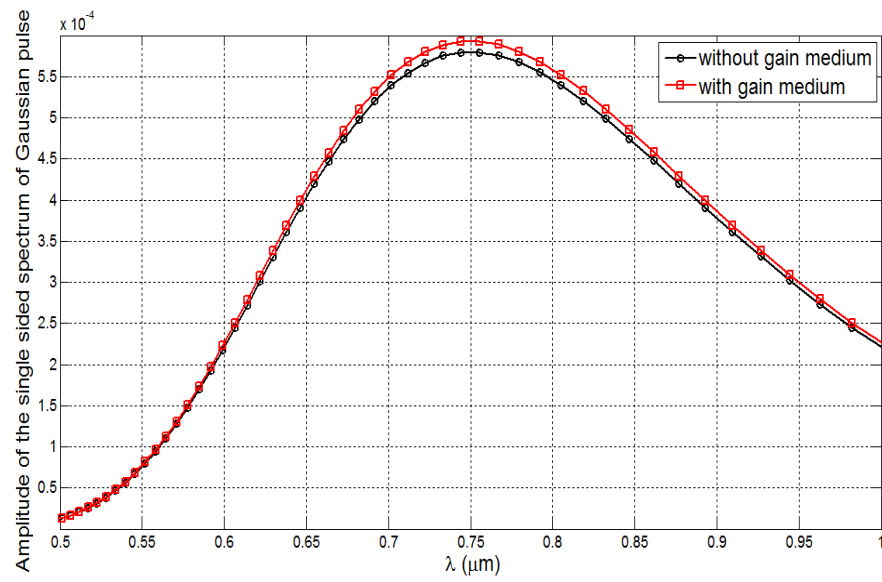


Figure 5.9: Low amplitude Gain spectrum at point after  $10\mu\text{m}$  distance inside the quantum well gain medium.

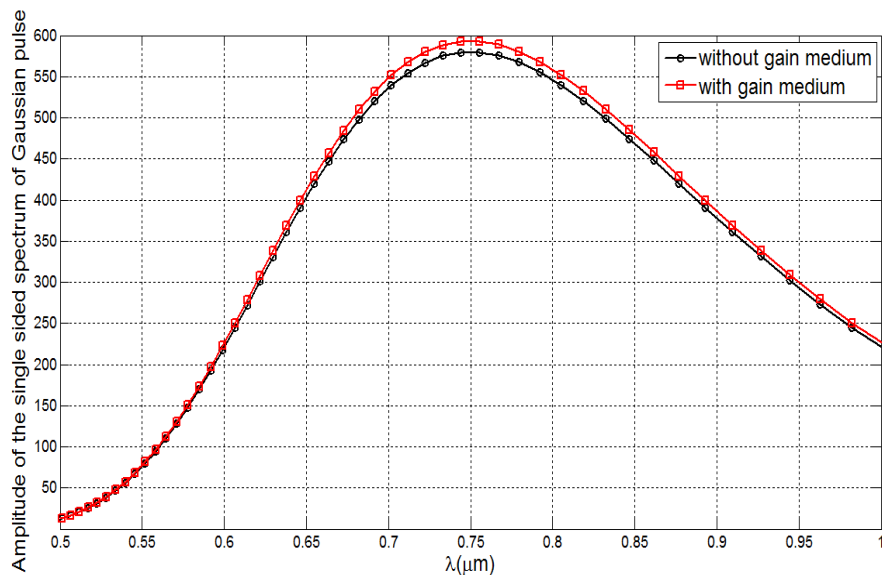


Figure 5.10: High amplitude Gain spectrum at point after  $10\mu\text{m}$  distance inside the quantum well gain medium.

As shown in figures(5.9,5.10) the amplification factor after a distance of  $10\mu\text{m}$  is found to be 1.023 which in agreement with results in [23].

## 5.2 Quantum Dash and Quantum Dot Results

### 5.2.1 Modeling Results

The rate equations(4.29,4.30) are run for 9ns with  $\Delta t = 10^{-15}s$  using the quantum dash/dot parameters mentioned in the paper [37] and these parameters are

Table 5.4: InAs/InP Quantum Dash parameters.

mass electron $m_e$ (kg)	9.11e-31
Effective mass of electron $m_o$ (kg)	$0.04m_e$
Refractive index of active region $n_r$ )	3.5
Number of Dash layers	4
Height of dash(nm)	1.5
Width of dash(nm)	20
Length of Cavity( $\mu\text{m}$ )	10
$\beta$	$1e - 4$
$D_g$	1
$D_w(m^{-3})$	$1.8e25$
$N_d(m^{-3})$	$5e23$
$\tau_{capo}(s)$	$2e - 12$
$E_{cv}$ (mev)	805
$\Delta E$ (mev)	0.354
Number of dash groups M	181
Number of modes	105
Number of intra Dash energylevels $k_{max}$	50
Pumping Current(mA)	56.1

listed in the table(5.4).

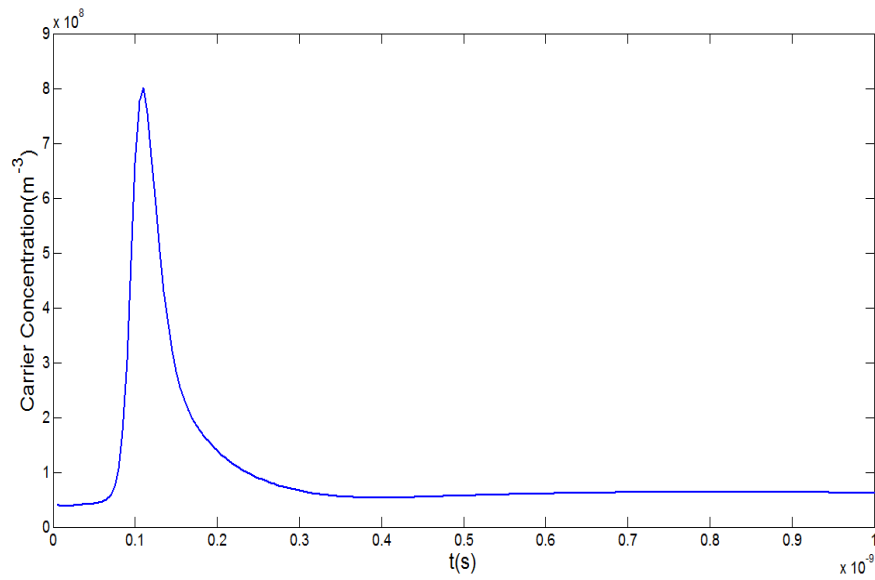


Figure 5.11: Carrier concentrations ( $N_w$ ) of wetting layer as function of time.

The energy diagram of wetting layer and different dash/dot groups are shown in figure(4.5). The change in the carrier concentration of the wetting layer  $N_w$  as function of time is shown in figure(5.11) above. The steady state is reached after 900fs.

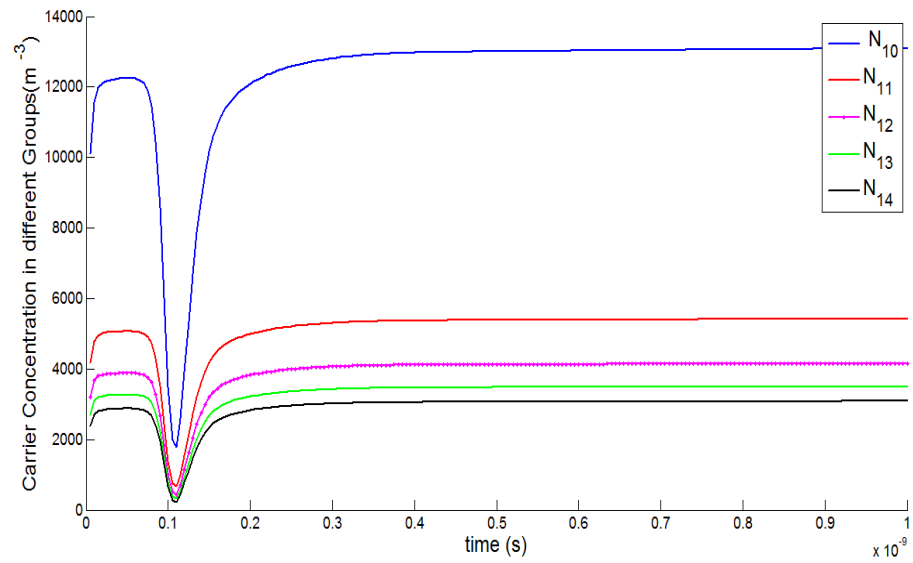


Figure 5.12: Carrier concentrations ( $N_{jk}$ ) of four different dash groups as function of time.

The carrier concentrations  $N_{jk}$  in four different dash groups as function of time is show in figure(5.12).

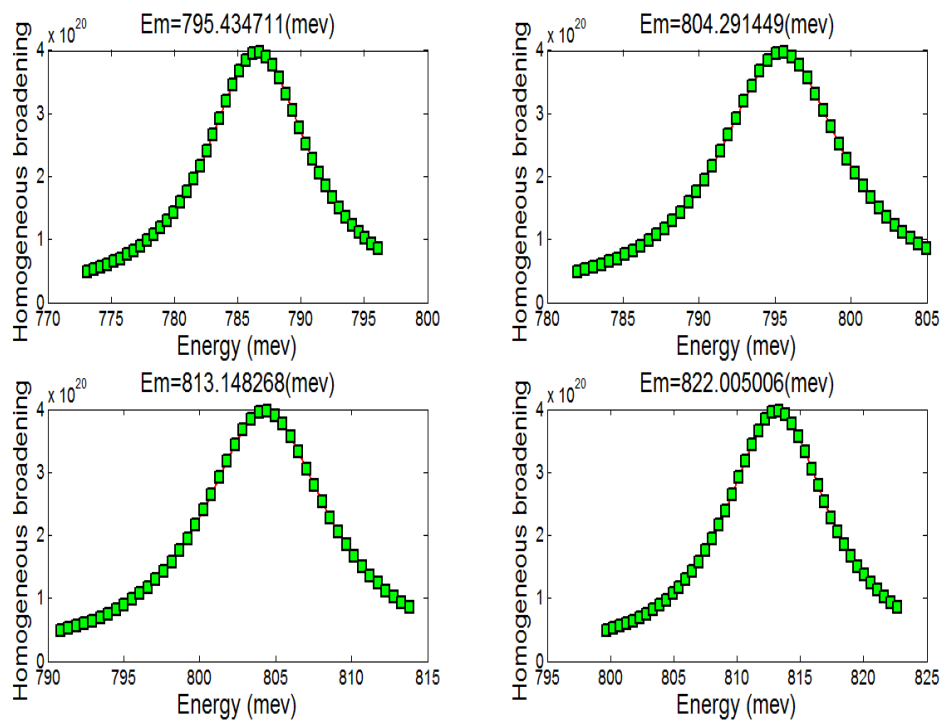


Figure 5.13: Homogeneous broadening of four different dash groups for all  $k$  ( $k = 0, 1, \dots, k_{max}$ ).

Homogeneous broadening in four different dash groups with central energy (mev) is show in figure(5.13)

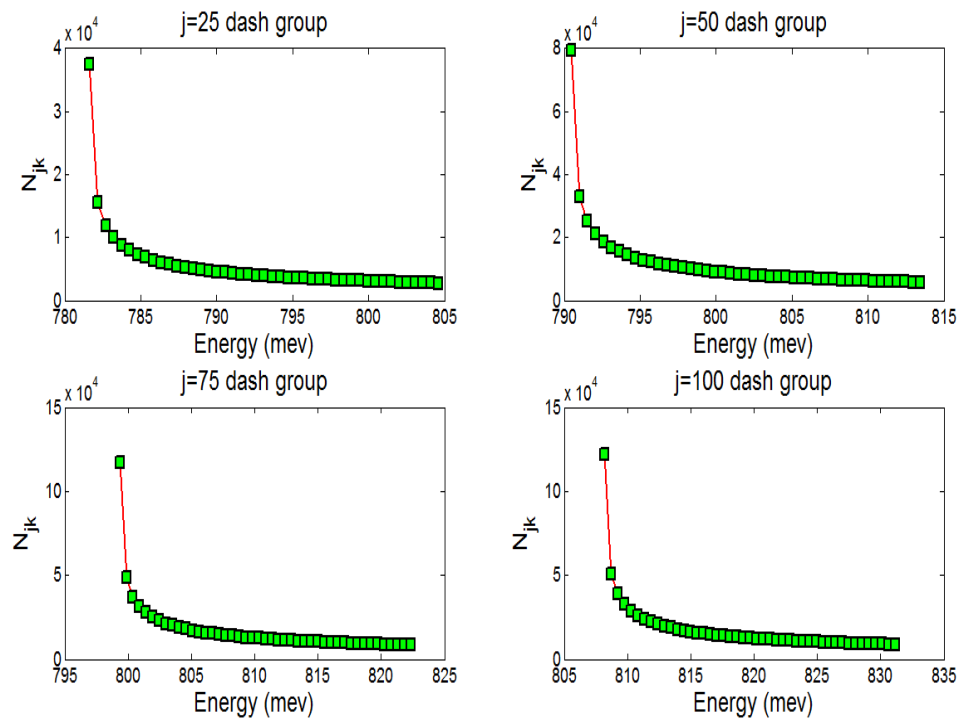


Figure 5.14: Carrier concentrations ( $N_{jk}$ ) of four different dash groups for all  $k$  ( $k = 0, 1, ..kmax$ ).

After steady state is reached, the carrier concentration of all intra dash energy levels (shown in figure(4.7)) of four different dash groups are shown in figure(5.14).

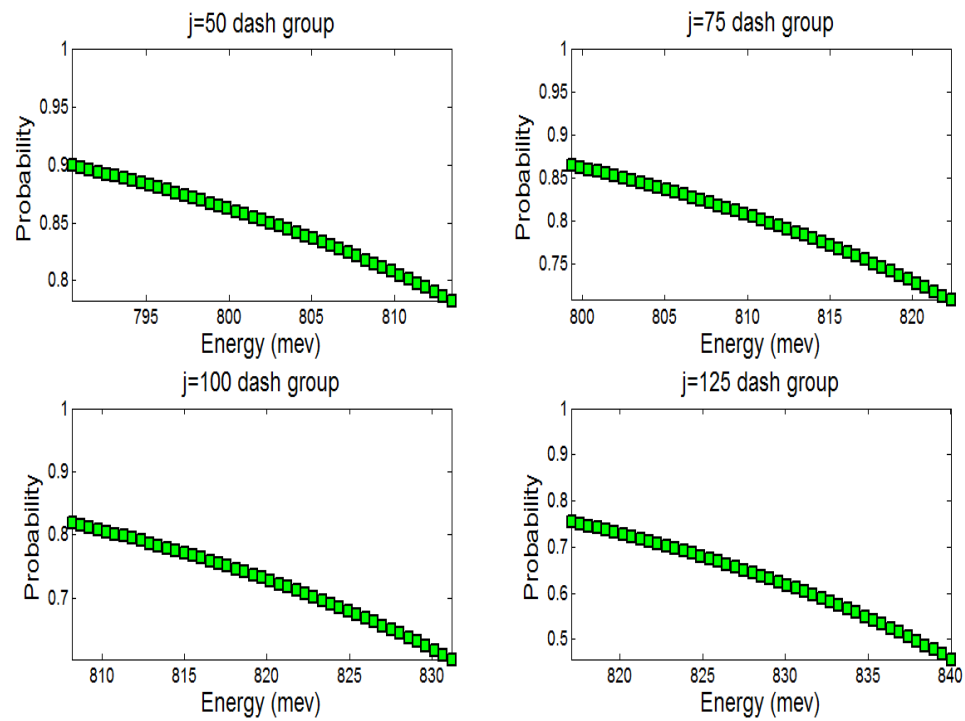


Figure 5.15: Probability of occupation ( $P_{jk}$ ) of four different dash groups for all  $k$  ( $k = 0, 1, \dots, k_{max}$ ).

The variations in the probability of occupation in four dash groups for all intra dash energy levels (shown in figure(4.7)) is depicted in figure(5.15).

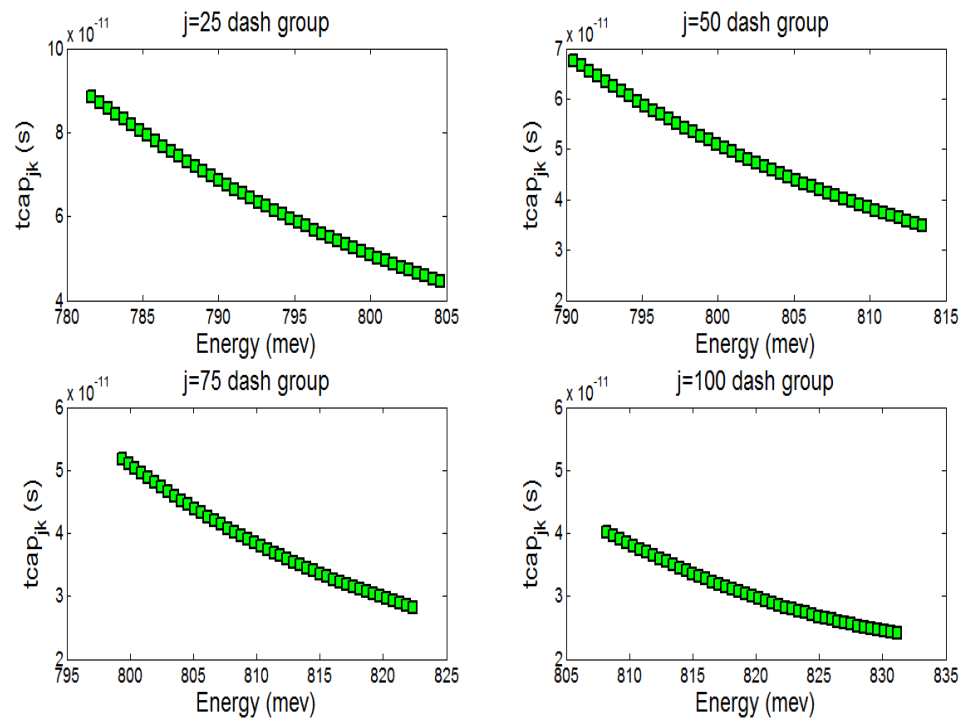


Figure 5.16: Capture time ( $t_{cap_{jk}}$ ) of four different dash groups for all  $k$  ( $k = 0, 1, \dots, k_{max}$ ).

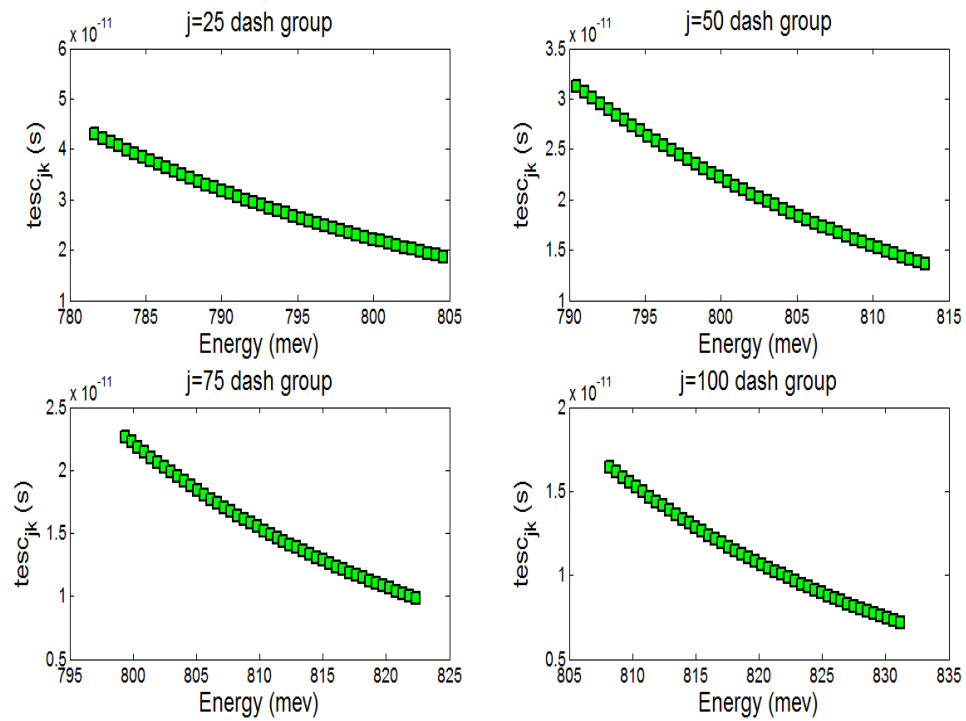


Figure 5.17: Escape time ( $t_{esc}^{jk}$ ) of four different dash groups for all  $k$  ( $k = 0, 1, \dots, kmax$ ).

Similarly the variation in the capture and escape time in four dash groups for all intra dash energy levels (shown in figure(4.7)) is explained in figures(5.16,5.17).

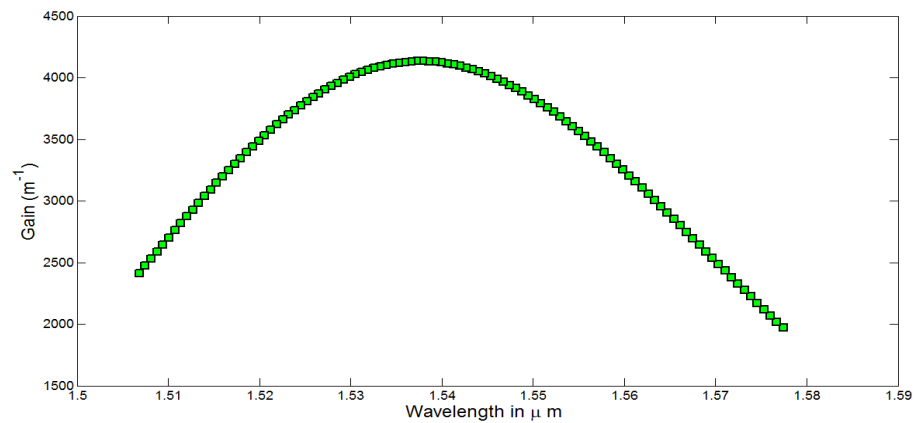


Figure 5.18: Steady state InAs/InP quantum dash gain vs wavelength.

The final gain of the quantum dash group ensemble is obtained as shown in figure(5.18). The gain obtained by this model is consistent with results presented in the paper [37; 58].

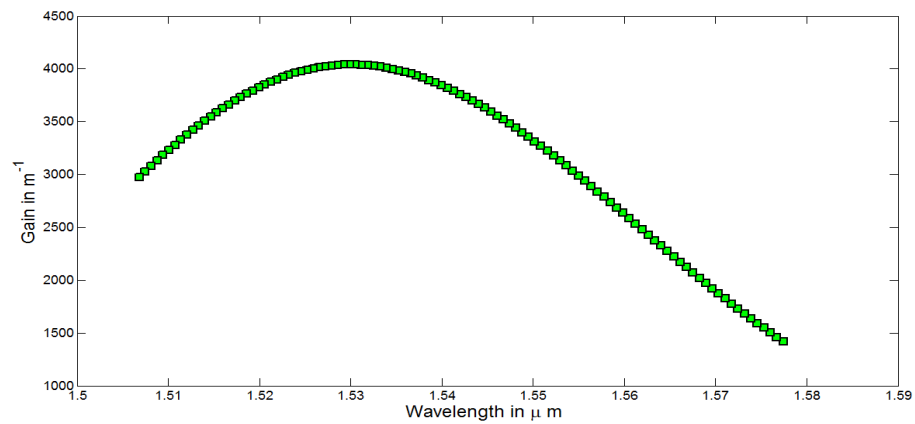


Figure 5.19: Steady state InAs/InP quantum dot gain vs wavelength.

In a similar way the final gain of the quantum dot group ensemble is obtained as shown in figure(5.19).

### 5.2.2 Fitting Lorentzian parameters

To fit the gain profile of InAs/InP quantum dash/dot to the Lorentzian parameters (a,b,c and d as shown in the table(5.5)) for the ADE-FDTD model, the gain profile obtained must be multiplied with a coupling factor before commencing the fitting procedure . In case of InAs/InP quantum dashes/dots the coupling factor is found to be  $coupFac = 3.124583194 \times 10^{-17}$  . For fitting the gain of quantum dash/dot ensemble to the Lorentzian parameters nonlinear curve fitting method 'lsqcurvefit' of the Matlab is used with 'TolFun', $10^{-200}$  and 'TolX', $10^{-200}$  to minimize the error.

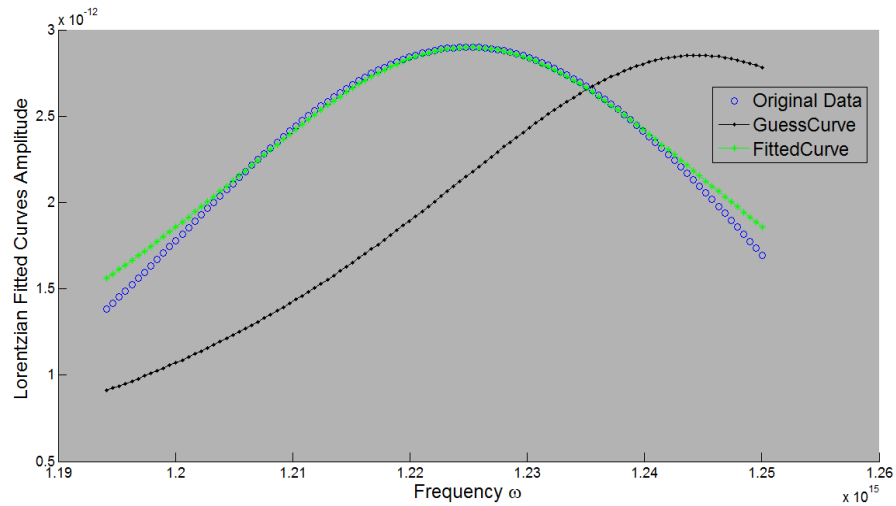


Figure 5.20: Fitting InAs/InP quantum dash steady state gain to the Lorentzian function.

The fitting results are explained in figure(5.20) above. The complex permittivity  $\epsilon_s = \epsilon_o\epsilon_r + \frac{a}{b+jc\omega-d\omega^2}$  can be determined once the fitting results are obtained. The real and imaginary parts of complex permittivity are shown in figure(5.21,5.22)

.

Table 5.5: Complex permittivity parameters for InAs/InP quantum dash.

$\epsilon_r$	$3.5^2$
a	$-1.090936 \times 10^{16}$
b	$1.55 \times 10^{30}$
c	$6.90000 \times 10^{13}$
d	1.0320385

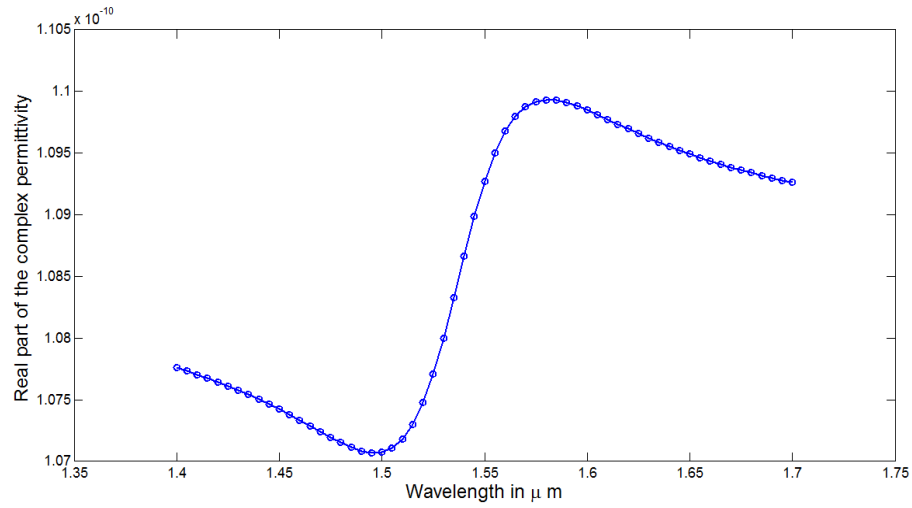


Figure 5.21: Real part of the complex permittivity of the quantum dash medium vs wavelength.

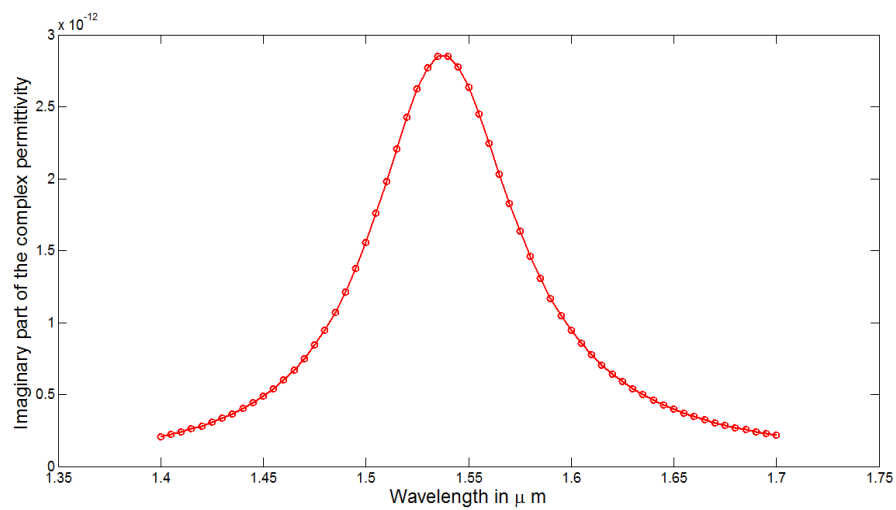


Figure 5.22: Imaginary part of the complex permittivity of the quantum dash medium vs wavelength.

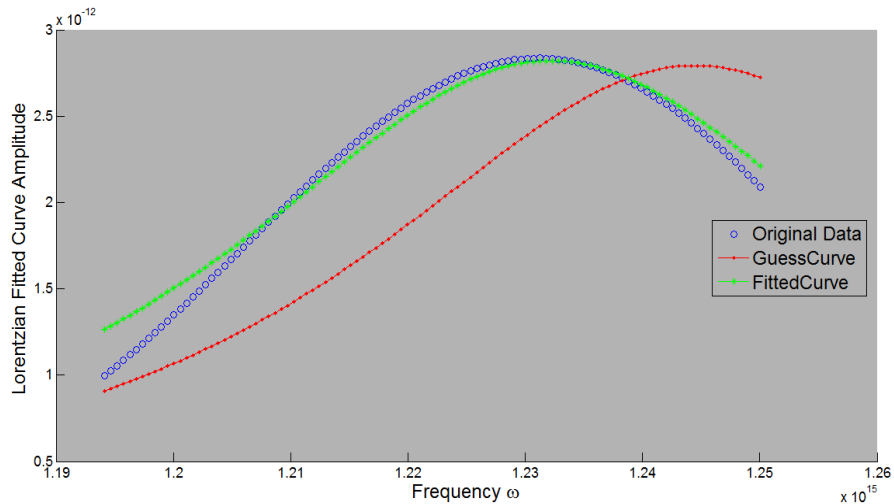


Figure 5.23: Fitting InAs/InP quantum dot steady state gain to the Lorentzian function.

Similarly the steady state gain expression of the InAs/InP quantum dot are obtained and fitted into the Lorentzian parameters and the results obtained are shown in figures(5.24,5.25).

Table 5.6: Complex permittivity parameters for InAs/InP quantum dot.

$\epsilon_r$	$3.5^2$
a	$-1.0820304 \times 10^{16}$
b	$1.55 \times 10^{30}$
c	$6.99000 \times 10^{13}$
d	1.020196

The real and imaginary parts of the complex permittivity for the InAs/InP quantum dots with the parameters mentioned in the table (5.6) are show in

figures(5.24,5.25).

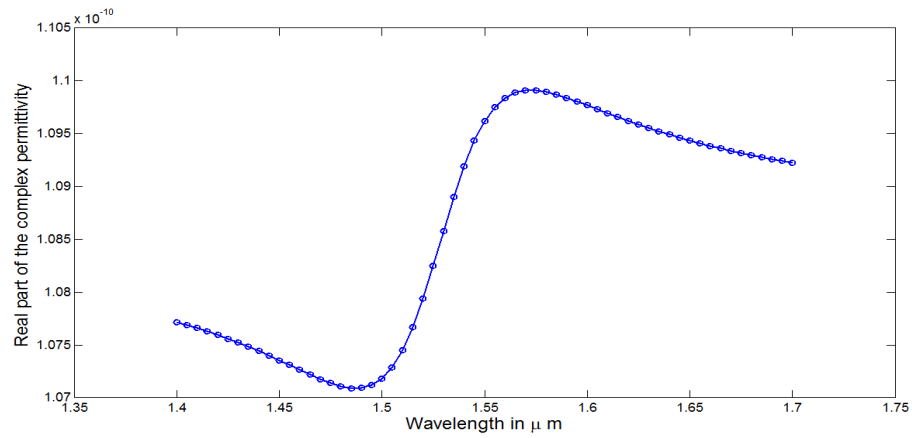


Figure 5.24: Real part of complex permittivity of quantum dot medium vs wavelength.

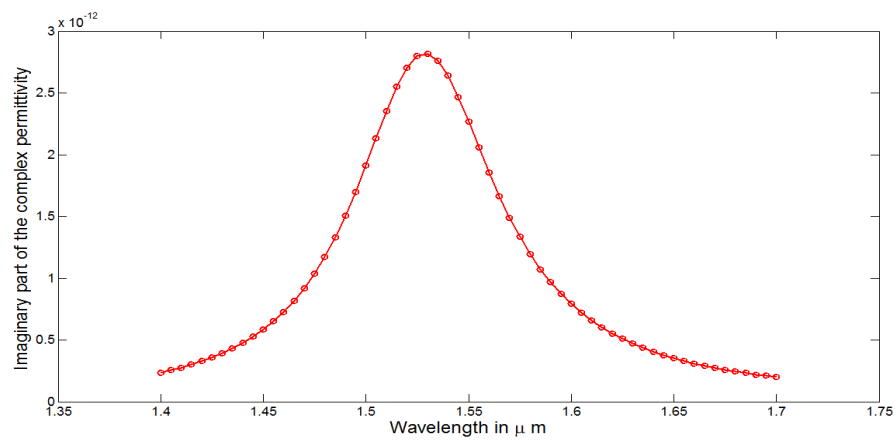


Figure 5.25: Real part of complex permittivity of quantum dot medium vs wavelength.

### 5.2.3 Dielectric waveguide

To analyze the gain properties, the quantum dash/dot gain medium is placed in a dielectric waveguide as shown in figure(5.26).

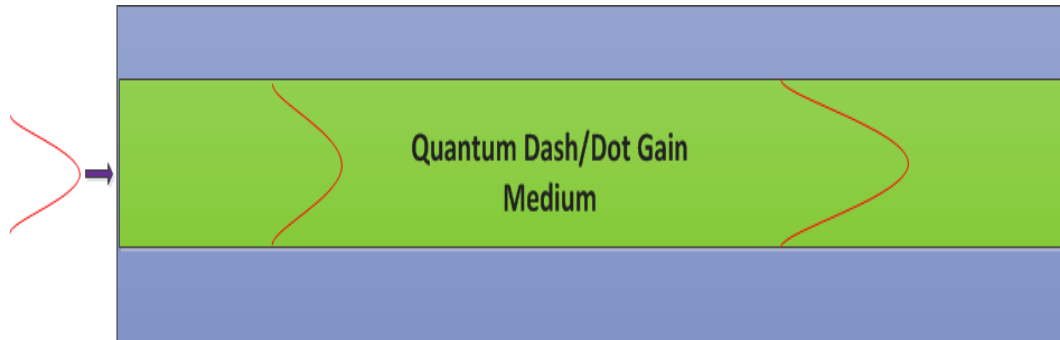


Figure 5.26: Dielectric waveguide with quantum Dash/Dot gain medium.

The mode (figure(5.27)) is multiplied with the frequency corresponding to the wavelength  $1.55\mu\text{m}$  to enter it into the waveguide.

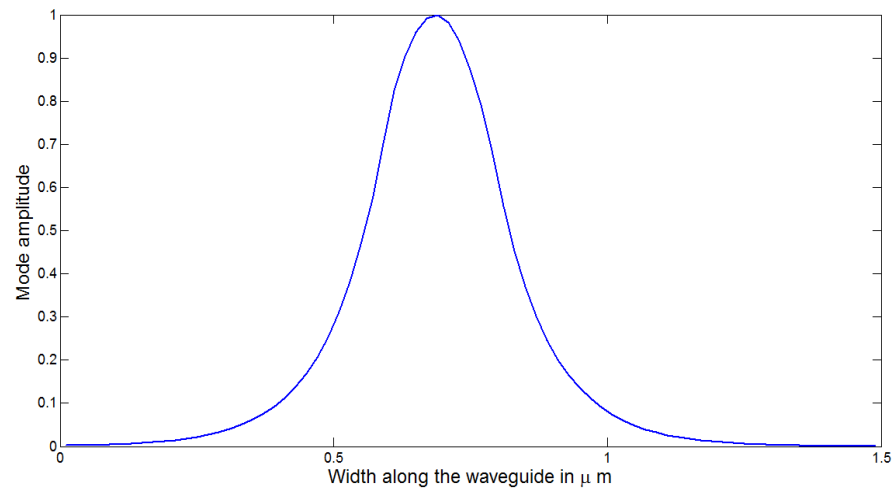


Figure 5.27: The mode which is inserted into the dielectric waveguides.

The pulses propagating in the gain medium (quantum dash/dot) are shown in figures (5.28,5.29)

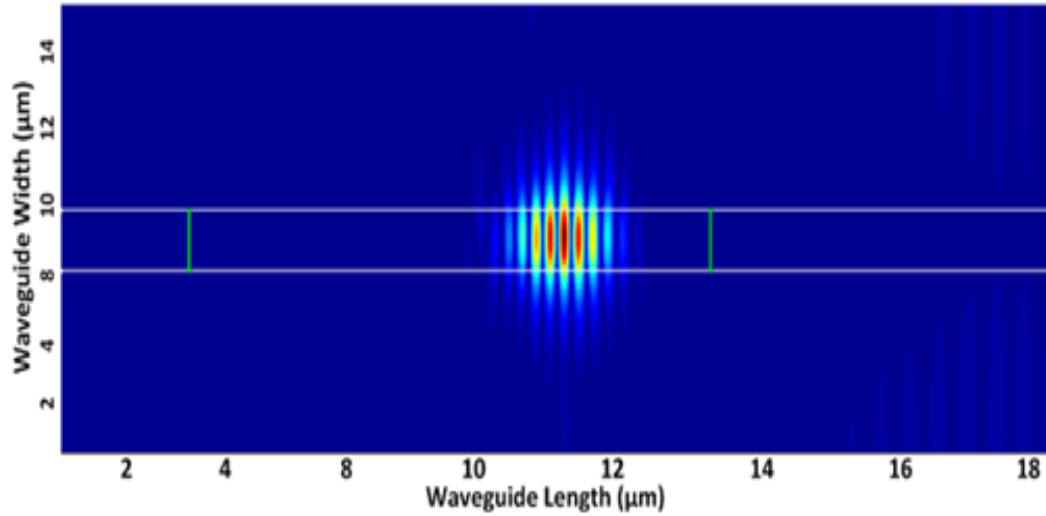


Figure 5.28: Gaussian pulse propagating in the dielectric waveguide with quantum dash gain medium of length  $10\mu\text{m}$ .

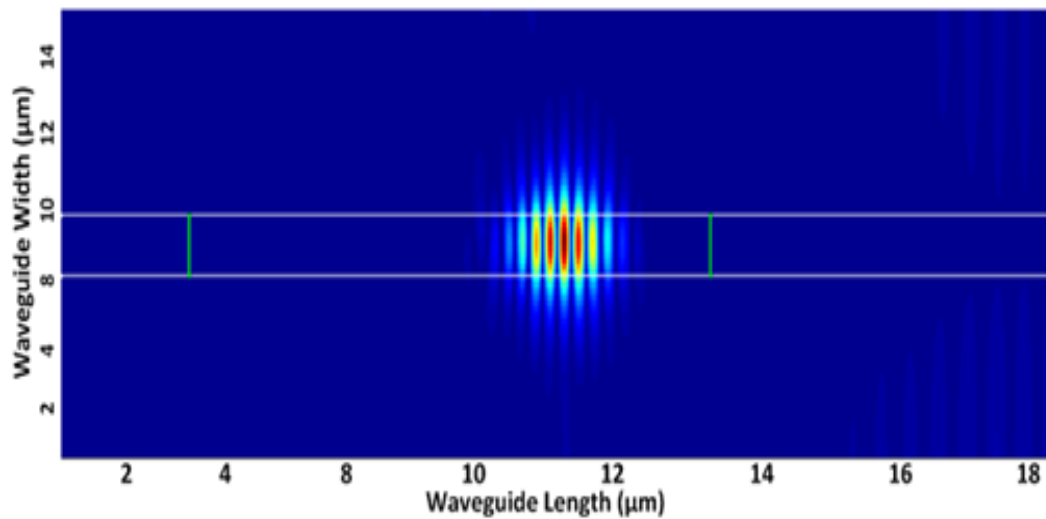


Figure 5.29: Gaussian pulse propagating in the dielectric waveguide with quantum dot gain medium of length  $10\mu\text{m}$ .

The electric fields inside the dielectric waveguide after traversing a distance of  $10\mu\text{m}$  in the gain medium (quantum dash/dot) is shown in figures(5.30,5.31)

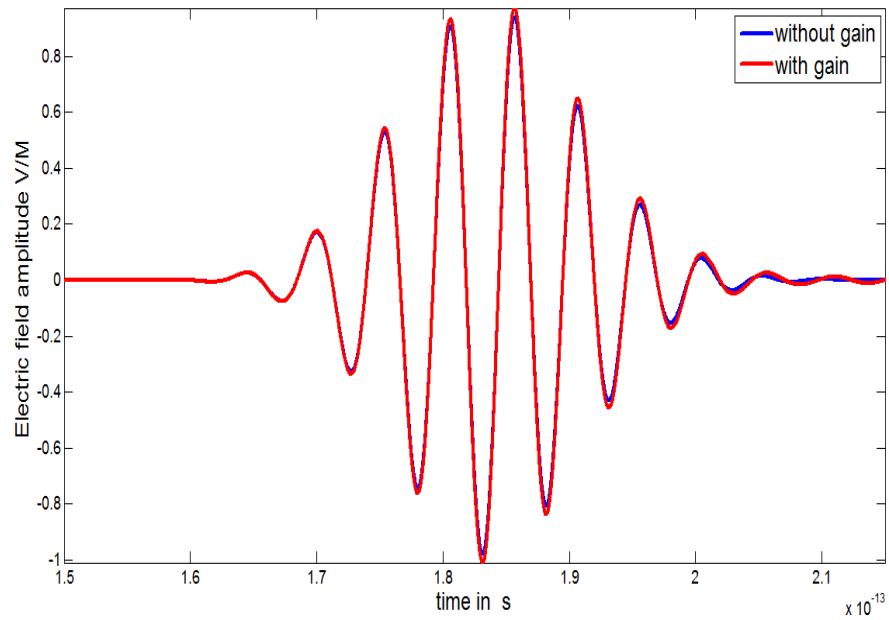


Figure 5.30: Gaussian pulse after traveling  $10\mu\text{m}$  distance with and without quantum dash gain medium.

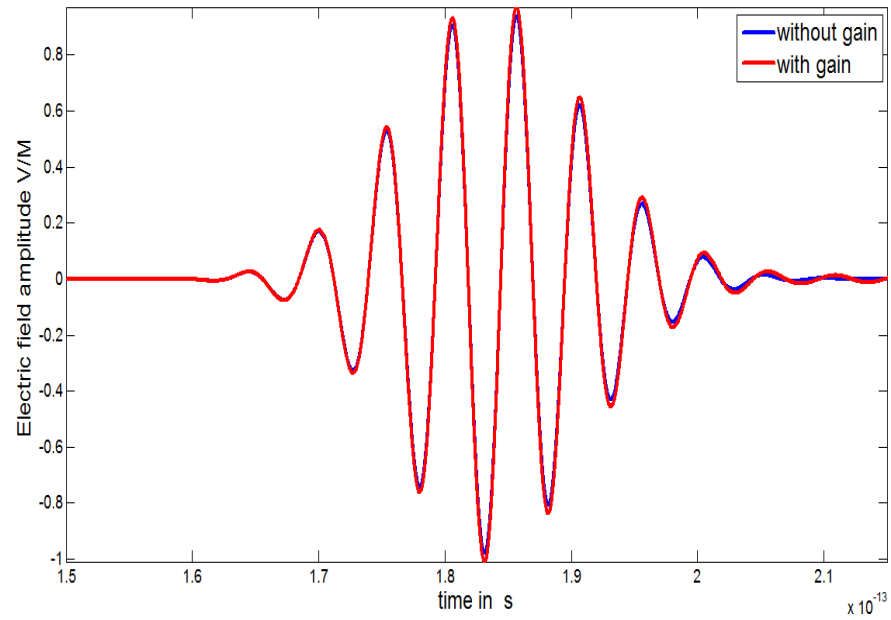


Figure 5.31: Gaussian pulse after traveling  $10\mu\text{m}$  distance with and without quantum dot gain medium.

The gain spectrum of the Gaussian pulse with and without gain medium (quantum dash/dot) are shown in figures (5.32,5.33).

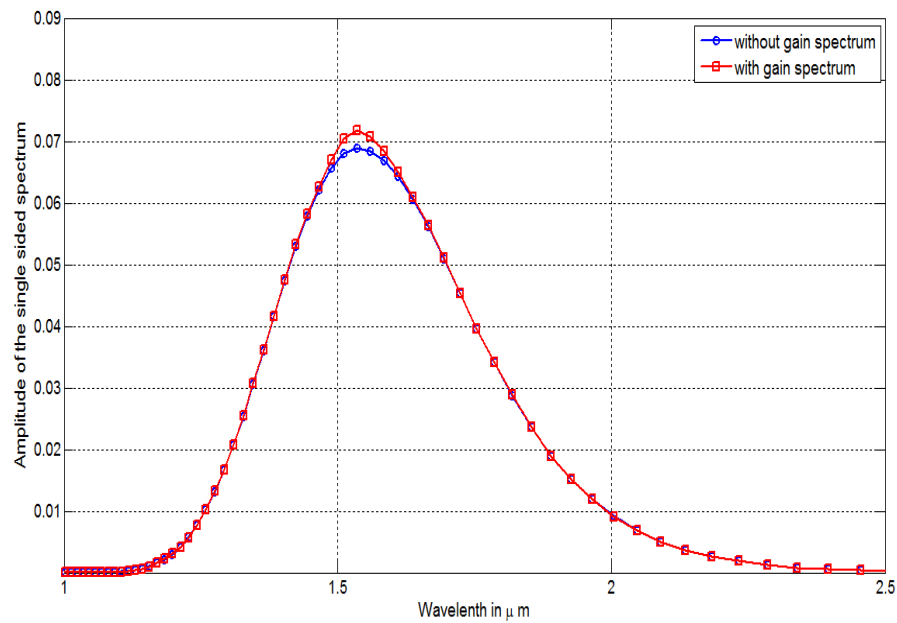


Figure 5.32: Frequency spectrum of the Gaussian pulse after traveling  $10\mu\text{m}$  distance, with and without the quantum dash gain medium.

The gain observed at the wavelength  $1.535\mu\text{m}$  in the spectrum (figure(5.32)) is  $1.04094$  or  $4094M^{-1}$  whereas the expected gain is  $1.04121$  (figure(5.18)). The error observed is  $0.026\%$  which is considerably very low and shows the accuracy of the model.

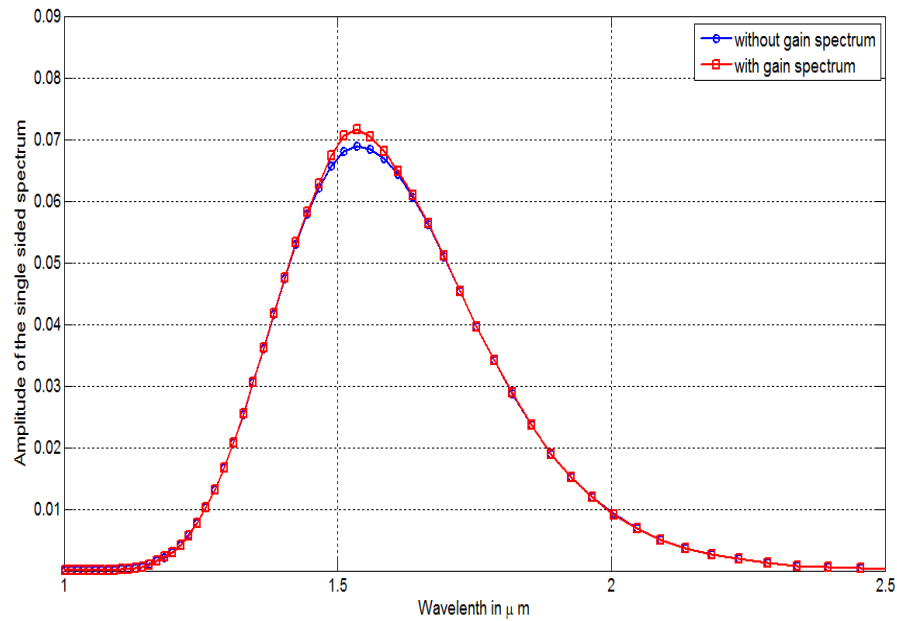


Figure 5.33: Frequency spectrum of the Gaussian pulse after traveling  $10\mu\text{m}$  distance, with and without the quantum dot gain medium.

Similarly in the case of quantum dot, the gain observed at  $1.535\mu\text{m}$  in the spectrum (figure(5.33)) is  $1.0397793$  or  $3977.93M^{-1}$  where as the expected gain is  $1.03998$  (figure(5.19)). The error percentage observed is  $0.019\%$  which is again very low.

# Chapter 6

## Conclusion and Future Work

## 6.1 Conclusion

Modeling of quantum dashes is complicated because of the number of parameters involved. ADE-FDTD implementation is even more complicated both computationally and conceptually. In this thesis we have attempted to model a simplified case of quantum dashes/dots using ADE-FDTD . ADE-FDTD modeling of quantum well using the general algorithm [38] is proposed and discussed. After developing the well model the method is extended to model the dynamics of InAs/InP quantum dots and quantum dashes. The ADE-FDTD small signal analysis of quantum dash/dots is done after allowing the carrier concentrations in all dash/dot groups to reach the steady state. In the well model the effect of the medium on the field and the effect of the field on the medium are considered. However in the modeling of dash/dot the focus of the thesis was to study the effect of the dash/dot medium on the field using small signals but not vice-versa. The important objectives achieved in the thesis are listed below

- Good amount of literature survey on the nature of Quantum Well, Quantum Dots and Quantum Dashes as gain media is presented.
- The rate equation modeling of Quantum Well, Quantum Dots and Quantum Dashes is analyzed and new algorithms are presented to model them

using the ADE-FDTD method.

- The formulated FDTD equations to include gain in the propagation media (Quantum Well, Quantum Dots and Quantum Dashes) using Auxiliary Differential Equation (ADE) and general algorithm [38] with two dimensional Maxwell's equations are studied extensively for the stability and efficiency.
- The developed multidimensional simulator is used to study and analyze time and frequency domain dynamics.
- Important conclusions were presented.

## 6.2 Future Work

In the thesis we have attempted to model quantum dashes/dots using a simple ADE-FDTD approach for small signal analysis by fitting the parameters involved using a Lorentzian function . The model can be improved by extending it to consider the effect of field on the carrier concentration of the dash/dot groups for the large signal analysis. This extension will require a greater conceptual understanding of dash/dot dynamic behavior and good amount of computational power to solve the number of equations involved in parallel. Once the model

is perfected it will be of very good use to study the dynamics of 1D and 0D quantum structures, which is of paramount importance in the photonic industry these days. The model can also be extended to study the optical dynamics in laser cavities.

# Bibliography

- [1] J. Hamm, “Spatio-temporal and polarisation dynamics of semiconductor microcavity lasers,” 2005.
- [2] J. Loehr, *Physics of strained quantum well lasers*. Kluwer Academic Publishers, 1998.
- [3] A. Tsatsulnikov, A. Kovsh, A. Zhukov, Y. Shernyakov, Y. Musikhin, V. Ustinov, N. Bert, P. Kopev, Z. Alferov, A. Mintairov, *et al.*, “Volmer–weber and stranski–krastanov inas-(al, ga) as quantum dots emitting at 1.3  $\mu\text{m}$ ,” *Journal of Applied Physics*, vol. 88, p. 6272, 2000.
- [4] A. Maslov and C. Ning, “Modal gain in a semiconductor nanowire laser with anisotropic bandstructure,” *Quantum Electronics, IEEE Journal of*, vol. 40, pp. 1389 – 1397, oct. 2004.

- [5] Y. Yamamoto and T. Mukai, “Fundamentals of optical amplifiers,” *Optical and Quantum Electronics*, vol. 21, pp. S1–S14, 1989. 10.1007/BF02117679.
- [6] F. Lelarge, B. Dagens, J. Renaudier, R. Brenot, A. Accard, F. van Dijk, D. Make, O. L. Gouezigou, J.-G. Provost, F. Poingt, J. Landreau, O. Drisse, E. Derouin, B. Rousseau, F. Pommereau, and G.-H. Duan, “Recent advances on inas/inp quantum dash based semiconductor lasers and optical amplifiers operating at 1.55  $\mu\text{m}$ ,” *Selected Topics in Quantum Electronics, IEEE Journal of*, vol. 13, pp. 111–124, jan.-feb. 2007.
- [7] J. Reithmaier, G. Eisenstein, and A. Forchel, “Inas/inp quantum-dash lasers and amplifiers,” *Proceedings of the IEEE*, vol. 95, pp. 1779–1790, sept. 2007.
- [8] P. Michler, *Single quantum dots: fundamentals, applications, and new concepts*, vol. 90. Springer, 2003.
- [9] T. Berg and J. Mork, “Saturation and noise properties of quantum-dot optical amplifiers,” *Quantum Electronics, IEEE Journal of*, vol. 40, pp. 1527–1539, nov. 2004.
- [10] P. Borri, W. Langbein, J. Hvam, F. Heinrichsdorff, M.-H. Mao, and D. Bimberg, “Spectral hole-burning and carrier-heating dynamics in ingaas

- quantum-dot amplifiers,” *Selected Topics in Quantum Electronics, IEEE Journal of*, vol. 6, pp. 544–551, may/jun 2000.
- [11] N. Matthew and O. Sadiku, “Numerical techniques in electromagnetics,” *CRC Press, USA*, 2001.
- [12] K. Yee, “Numerical solution of initial boundary value problems involving maxwell’s equations in isotropic media,” *Antennas and Propagation, IEEE Transactions on*, vol. 14, no. 3, pp. 302–307, 1966.
- [13] A. Taflove and S. Hagness, *Computational electrodynamics*. Artech house Boston, 1995.
- [14] M. Henini and M. Bugajski, “Advances in self-assembled semiconductor quantum dot lasers,” *Microelectronics journal*, vol. 36, no. 11, pp. 950–956, 2005.
- [15] W. Buhro and V. Colvin, “Shape matters,” *Nature materials*, vol. 2, no. 3, pp. 138–139, 2003.
- [16] R. Dingle and C. Henry, “Quantum effects in heterostructure lasers,” Sept. 21 1976. US Patent 3,982,207.
- [17] Y. Arakawa, “Progress in growth and physics of nitride-based quantum dots,” *Nano-Optoelectronics*, pp. 391–410, 2002.

- [18] H. Goronkin, P. Von Allmen, R. Tsui, and T. Zhu, “Functional nanoscale devices,” *Nanostructure Science and Technology*, p. 67, 1999.
- [19] Y. Arakawa and H. Sakaki, “Multidimensional quantum well laser and temperature dependence of its threshold current,” *Applied Physics Letters*, vol. 40, no. 11, pp. 939–941, 1982.
- [20] A. S. Nagra, S. Member, and R. A. York, “FDTD Analysis of Wave Propagation in Nonlinear Absorbing and Gain Media,” *Office*, vol. 46, no. 3, pp. 334–340, 1998.
- [21] R. Member, “FDTD Simulation of Femtosecond Optical Gating in Nonlinear Optical Waveguide Utilizing Intersubband Transition in AlGa<sub>N</sub> / Ga<sub>N</sub> Quantum Wells,” *Society*, vol. 0, no. 6, pp. 981–988, 2000.
- [22] S. Shi, B. Redding, T. Creazzo, E. Marchena, and D. W. Prather, “Quantum Electrodynamics Modeling of Silicon-Based Active Devices,” *Advances in Optical Technologies*, vol. 2008, pp. 1–11, 2008.
- [23] B. Redding, S. Shi, T. Creazzo, and D. W. Prather, “Electromagnetic modeling of active silicon nanocrystal waveguides,” *Optics Express*, vol. 16, no. 12, pp. 8792–8799, 2008.
- [24] S. Shi and D. W. Prather, “Lasing dynamics of a silicon photonic crystal microcavity,” *Optics Express*, vol. 15, no. 16, pp. 10294–10302, 2007.

- [25] S. V. Zhukovsky and D. N. Chigrin, “Numerical modelling of lasing in microstructures,” vol. 3527, no. 10, pp. 3515 – 3527, 2007.
- [26] G. Slavcheva, J. M. Arnold, and R. W. Ziolkowski, “Ultrashort Pulse Lossless Propagation Through a Degenerate Three-Level Medium in Nonlinear Optical Waveguides and Semiconductor Microcavities,” *Quantum*, vol. 9, no. 3, pp. 929–938, 2003.
- [27] T. Matsui, “Numerical Simulation of Lasing Dynamics in Cholesteric Liquid Crystal Based on ADE-FDTD Method,” 1995.
- [28] K. Böhringer and O. Hess, “A full-time-domain approach to spatio-temporal dynamics of semiconductor lasers. I. Theoretical formulation,” *Progress in Quantum Electronics*, vol. 32, pp. 159–246, Jan. 2008.
- [29] L. Livermore, “Lasing in tilted-waveguide semiconductor laser amplifiers,” *Optical and Quantum Electronics*, vol. 26, pp. 207–217, 1994.
- [30] W. H. P. Pernice, F. P. Payne, and D. F. G. Gallagher, “A Finite-Difference Time-Domain Method for the Simulation of Gain Materials With Carrier Diffusion in Photonic Crystals,” *Lightwave*, vol. 25, no. 9, pp. 2306–2314, 2007.
- [31] I.-k. Hwang and Y.-h. Lee, “Nonlinear dispersive three-dimensional finite-

- difference time-domain analysis for photonic-crystal lasers,” *Optics Express*, vol. 13, no. 24, pp. 9645–9651, 2005.
- [32] Y. Zhang, W. Zheng, Q. Aiyi, H. Qu, H. Peng, S. Xie, and L. Chen, “Design of Photonic Crystal Semiconductor Optical Amplifier With Polarization Independence,” *Lightwave*, vol. 28, no. 22, pp. 3207–3211, 2010.
- [33] L. Coldren, S. Corzine, and L. Coldren, “Diode lasers and photonic integrated circuits,” 1995.
- [34] A. Sakamoto and M. Sugawara, “Theoretical Calculation of Lasing Spectra of Quantum-Dot Lasers : Effect of Homogeneous Broadening of Optical Gain,” *Technology*, vol. 12, no. 2, pp. 1999–2001, 2000.
- [35] A. Bilenca and G. Eisenstein, “On the noise properties of linear and nonlinear quantum-dot semiconductor optical amplifiers: The impact of inhomogeneously broadened gain and fast carrier dynamics,” *Quantum Electronics, IEEE Journal of*, vol. 40, no. 6, pp. 690–702, 2004.
- [36] D. Hadass, A. Bilenca, and R. Alizon, “Gain and noise saturation of wide-band InAs-InP quantum dash optical amplifiers: Model and experiments,” *Topics in Quantum*, vol. 11, no. 5, pp. 1015–1026, 2005.
- [37] Z. M. Khan, T. K. Ng, and B. S. Ooi, “Characteristics of Quantum Dash

- Laser under the Rate Equation Model Framework,” *Quantum*, pp. 65–66, 2010.
- [38] A. Al-Jabr and M. Alsunaidi, “A general ade-fdtd algorithm for the simulation of different dispersive materials,” *Session 1P8*, p. 111.
- [39] P. Zory, *Quantum well lasers*. Academic Pr, 1993.
- [40] A. Zilkie, J. Meier, M. Mojahedi, P. Poole, P. Barrios, D. Poitras, T. Rotter, C. Yang, A. Stintz, K. Malloy, P. Smith, and J. Aitchison, “Carrier dynamics of quantum-dot, quantum-dash, and quantum-well semiconductor optical amplifiers operating at 1.55  $\mu\text{m}$ ,” *Quantum Electronics, IEEE Journal of*, vol. 43, pp. 982–991, nov. 2007.
- [41] A. Dissertation, “NORTHWESTERN UNIVERSITY FDTD Computational Electromagnetics Modeling of Microcavity Lasers and Resonant Optical Structures,” no. June, 1998.
- [42] R. Luebbers, F. Hunsberger, K. Kunz, R. Standler, and M. Schneider, “A frequency-dependent finite-difference time-domain formulation for dispersive materials,” *Electromagnetic Compatibility, IEEE Transactions on*, vol. 32, no. 3, pp. 222–227, 1990.
- [43] R. Joseph, S. Hagness, and A. Taflove, “Direct time integration of maxwells

equations in linear dispersive media with absorption for scattering and propagation of femtosecond electromagnetic pulses,” *Optics Letters*, vol. 16, no. 18, pp. 1412–1414, 1991.

- [44] T. F.-d. T.-d. Method, A. Taflove, and S. C. Hagness, *Computational Electrodynamics Third Edition*.
- [45] T. Namiki, “A New FDTD Algorithm Based,” *October*, vol. 47, no. 10, pp. 2003–2007, 2003.
- [46] P. Petropoulos, “Stability and phase error analysis of FD-TD in dispersive dielectrics,” *IEEE Transactions on Antennas and Propagation*, vol. 42, no. 1, pp. 62–69, 1994.
- [47] W. Pernice, F. Payne, and D. Gallagher, “An fdtd method for the simulation of dispersive metallic structures,” *Optical and quantum electronics*, vol. 38, no. 9, pp. 843–856, 2006.
- [48] P. Suter and T. Graf, “Photothermal thickness measurement of multilayered structures: An experimental and numerical analysis,” *Journal of Applied Physics*, vol. 103, p. 033509, 2008.
- [49] W. Chow, S. Koch, and M. Sargent III, *Semiconductor-laser physics*. Springer-Verlag New York, Inc., 1994.

- [50] G. Eisenstein, U. Koren, G. Raybon, T. Koch, J. Wiesenfeld, M. Wegener, R. Tucker, and B. Miller, “Large-and small-signal gain characteristics of 1.5  $\mu\text{m}$  multiple quantum well optical amplifiers,” *Applied physics letters*, vol. 56, no. 13, pp. 1201–1203, 1990.
- [51] D. Bimberg, M. Grundmann, and N. Ledentsov, *Quantum dot heterostructures*. Wiley, 1999.
- [52] Y. Nambu, A. Tomita, H. Saito, and K. Nishi, “Effects of spectral broadening and cross relaxation on the gain saturation characteristics of quantum dot laser amplifiers,” *Japanese journal of applied physics*, vol. 38, p. 5087, 1999.
- [53] T. Akiyama, H. Kuwatsuka, T. Simoyama, Y. Nakata, K. Mukai, M. Sugawara, O. Wada, and H. Ishikawa, “Application of spectral-hole burning in the inhomogeneously broadened gain of self-assembled quantum dots to a multiwavelength-channel nonlinear optical device,” *Photonics Technology Letters, IEEE*, vol. 12, no. 10, pp. 1301–1303, 2000.
- [54] D. Hadass, A. Bilenca, R. Alizon, S. Member, and G. Eisenstein, “Gain and noise saturation of wide-band InAs-InP quantum dash optical amplifiers: Model and experiments,” *Topics in Quantum*, vol. 11, no. 5, pp. 690–702, 2004.

- [55] D. Deppe and D. Huffaker, “Quantum dimensionality, entropy, and the modulation response of quantum dot lasers,” *Applied Physics Letters*, vol. 77, p. 3325, 2000.
- [56] M. Sugawara, *Self-assembled InGaAs/GaAs quantum dots*, vol. 60. Academic Pr, 1999.
- [57] M. Gioannini, “Effect of wetting-layer and barrier states on the optical gain characteristics of a qdash waveguide for ecl tunable laser application,” 2004.
- [58] M. Z. M. Khan, T. K. Ng, U. Schwingenschlogl, P. Bhattacharya, B. S. Ooi, and S. Member, “Spectral Analysis of Quantum Dash Lasers : Effect of Inhomogeneous Broadening of the Active Gain Region,” pp. 1–7.

# Curriculum Vitae

## **Javeed Ali Khan Mohammed**

- Born in Hyderabad, India on August 20, 1987.
- Received Bachelor of Engineering (BE) degree in 2008 from Muffakham Jah College of Engineering and Technology (MJCET) affiliated to Osmania University, Hyderabad, India.
- Worked in Accenture from June 2008 to Feb 2010.
- Joined King Fahd University of Petroleum and Minerals (KFUPM) in February 2010 as a Research Assistant in Electrical Engineering Department.
- Completed Master of Science(M.S) degree in Electrical Engineering with 3.88/4 GPA from KFUPM in April 2012.

**Contact details:**

- **Present Address:** Department of Electrical, King Fahd University of Petroleum and Minerals, P.O. Box , Dhahran 31261, Saudi Arabia.
- **E-mail Address:** jaavedkhan@kfupm.edu.sa, jaaved9.khan@gmail.com
- **Permanent Address:**18-8-244/C/39/A,Hyderabad-500023, India.